

EVOLUTIONARY STUDIES INSTITUTE AND SCHOOL OF GEOSCIENCES,
UNIVERSITY OF THE WITWATERSRAND

The functional morphology and internal structure of the forelimb of the Early Triassic non- mammaliaform cynodont *Thrinaxodon liorhinus*

Master's Dissertation

Safiyyah Iqbal

5/6/2015

Supervisors:

Dr. Kristian Carlson

Dr. Fernando Abdala



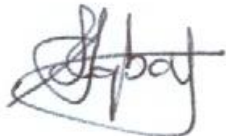
Student Number: 360821

DECLARATION

I, Safiyyah Iqbal (Student number: 360821), am a student registered for the degree in Master of Science by Dissertation (SR000) in the academic year 2014 completing in January 2015. I herewith submit the following research “The functional morphology and internal structure of the forelimb of the Early Triassic mammal-like cynodont *Thrinaxodon liorhinus*” in fulfillment of the requirements of the above course.

I hereby declare the following:

- I am aware that plagiarism (the use of someone else’s work without their permission and/or without acknowledging the original source) is wrong.
- I confirm that the work submitted for assessment for the above degree is my own unaided work except where I have explicitly indicated otherwise.
- This research has not been submitted before, either individually or jointly, for any course requirement, examination or degree at this or any other tertiary educational institution.
- I have followed the required conventions in referencing the thoughts and ideas of others.
- I understand that the University of the Witwatersrand may take disciplinary action against me if it can be shown that this task is not my own unaided work or that I failed to acknowledge the sources ideas or words in my writing in this research.



Signature: _____

Date: 06 May 2015

TABLE OF CONTENTS:

Declaration	Page 2
Table of Contents	Page 3
List of Tables and Figures	Page 4
List of Abbreviations	Page 5
Abstract	Page 6
Keywords	Page 6
Introduction	Page 7
Materials and Methods	
Materials	Page 10
Methods	Page 13
Muscle attachment sites	Page 19
Results	
Geometric morphometric landmark-based analyses	Page 19
Humerus	Page 20
Radius	Page 23
Ulna	Page 26
Indices	Page 29
Cortical thickness	Page 34
Torsion	Page 40
Discussion	
General configuration	Page 41
Internal morphology	Page 45
Limitations	Page 45
Conclusion	Page 46
Acknowledgments	Page 47
References	Page 48
Appendix 1	Page i
Appendix 2	Page xi
Appendix 3	Page xiii

LIST OF TABLES AND FIGURES:

Table 1: Sample composition	Page 11
Table 2: Scan parameters	Page 14
Figure 1: Measurements of indices	Page 15
Table 3: Scale factor	Page 17
Figure 2: Humeral PC1	Page 21
Figure 3: Humeral PC1 displacement	Page 21
Figure 4: Humeral PC2	Page 22
Figure 5: Humeral PC2 displacement	Page 22
Figure 6: Radial PC1	Page 24
Figure 7: Radial PC1 displacement	Page 24
Figure 8: Radial PC2	Page 25
Figure 9: Radial PC2 displacement	Page 25
Figure 10: Ulnae PC1	Page 27
Figure 11: Ulnae PC1 displacement	Page 27
Figure 12: Ulnae PC2	Page 28
Figure 13: Ulnae PC2 displacement	Page 28
Table 4: Regression	Page 29
Figure 14: SMI	Page 30
Figure 15: HRI	Page 31
Figure 16: EI	Page 32
Figure 17: IFA	Page 33
Figure 18: URI	Page 34
Figure 19: %Ct.Ar.	Page 35
Figure 20: $\ln I_x$ and $\ln I_y$	Page 36
Figure 21: $\ln I_x$ and $\ln I_y$	Page 37
Figure 22: I_x/I_y and I_{\max}/I_{\min}	Page 38
Figure 23: J	Page 39
Figure 24: J/2	Page 40
Figure 25: Torsion	Page 41

LIST OF ABBREVIATIONS

AZ	–	Assemblage Zone
MA	–	Millions of years ago
ESI	–	Evolutionary Studies Institute
APES	–	Animal, Plant and Environmental Sciences
SAS	–	School of Anatomical Sciences
DNMNH	–	Ditsong National Museum of Natural History
MCZ	–	Museum of Comparative Zoology
ANWC	–	Australian National Wildlife Collection
QM	–	Queensland Museum
TM	–	Tasmanian Museum
Sp.	–	Species
CT	–	Computed Tomography
SMI	–	Shoulder Moment Index
DLH	–	Deltoid Length of Humerus
HL	–	Humeral Length
HRI	–	Humerus Robustness Index
TDH	–	Transverse Diameter of Humerus
EI	–	Epicondyle Index
DEH	–	Epicondylar Width of Humerus
IFA	–	Index of Fossorial Ability
OL	–	Olecranon Length
FUL	–	Functional Ulna Length
URI	–	Ulna Robustness Index
TDU	–	Transverse Diameter of Ulna
Ps. Ar.	–	Periosteal Area
Ct. Ar.	–	Cortical Area
AP	–	Anteroposterior
ML	–	Mediolateral
Θ	–	Principal Angle
%Ct. Ar.	–	Percentage Cortical Area
J	–	Polar Moment of Area
J/2	–	Bending Rigidity
GM	–	Geometric Morphometric
PCA	–	Principal Component Analyses
PC	–	Principal Component
DF	–	Degrees of Freedom
n	–	Sample size
.stl	–	Stereolithography
.ver	–	Version description file format

Abstract

Thrinaxodon liorhinus, a cynodont that has been of captivating importance in the evolution of therapsids, is one of the best known transitional fossil taxa from non-mammaliaform cynodonts to mammals. The species is abundant in the South African Karoo Basin and is one of the best represented taxa immediately after the Permian-Triassic mass extinction. One of the key adaptive characteristics that may have aided in their survival was fossorialism. Numerous fossils of *Thrinaxodon* have been found in burrows or in a curled-up position, which has provided important circumstantial evidence for the formalization of the hypothesis of *Thrinaxodon* as a burrower. However, finding a fossil inside a burrow or even in a curled-up position only provides firm evidence for burrow use, not for burrow creation. Direct evidence for burrowing capability can come from the understanding of the functional morphology of *Thrinaxodon* limbs. The present study investigates internal and external structure of the *Thrinaxodon* forelimb, a variety of reptiles characterized by different behavioural patterns, and other cynodonts in order to advance present knowledge about the functional morphology of the transitional phase cynodont. The study uses Geometric Morphometric analyses, forelimb metric indices, torsion and cortical thickness of humeri in order to determine the extent to which, the *Thrinaxodon* forelimb functionally and structurally resembles that of a fossorial mammal versus a digging reptile. Results of the study tease apart the extent to which the *Thrinaxodon* forelimb illustrates modifications due to gait (e.g., sprawling versus semi-sprawling) versus a fossorial lifestyle. This would indicate that *Thrinaxodon* retained the reptilian skeletal configuration and adapted a posture that had begun to resemble parasagittal more than sprawling or semi-sprawling gait. Nonetheless, *Thrinaxodon* exhibits forelimb structural similarities to digging species, whether mammals or reptiles.

Keywords: Cross-sectional properties, fossorial lifestyle, geometric morphometric, muscle attachments, sprawling posture.

Introduction

Cynodonts, members of the mammal-like therapsid lineage, are first documented in the Late Permian and include mammals as the only living group (Kemp 2005). Cynodonts are the youngest therapsid group whose main diversification occurred in the Triassic (Abdala and Ribeiro 2010). Non-mammaliaform cynodonts (fossil members of the group closely related to mammals) are acknowledged as documenting one of the best transformational sequences in the fossil record, showing the acquisition of several key mammalian characteristics (Kemp 1983; Hopson 1987; Luo and Crompton 1994; Rubidge and Sidor 2001; Sidor and Smith 2004; Botha *et al.* 2004, 2007; Abdala and Ribeiro 2010). Features that evolve in these fossils that are present in today's mammals are the enlargement of the masseteric fossa in the lower jaw, development of a complete secondary osseous palate and double occipital condyle, among others (Kemp 2005).

The Beaufort Group of the Karoo Basin in South Africa is well-known for having the most complete record of non-mammaliaform cynodonts in a successive sequence going from Late Permian to the Middle Triassic (Kemp 1983; Botha *et al.* 2004, 2007). This geologic unit contains diverse and abundant fossils that enhance our understanding of Permian-Triassic palaeocommunities (Rubidge 1995, 2005). The earliest cynodont appears in the *Tropidostoma* Assemblage Zone (AZ) of the Karoo, while three genera have been found in the *Dicynodon* AZ at the end of the Permian, and four are documented after the Permian-Triassic extinction event (Abdala and Ribeiro 2010). The oldest evidence of cynodont burrowing has been found in the Lower Triassic of South Africa and has been attributed to *Thrinaxodon* (Damiani *et al.* 2003; Fernandez *et al.* 2013).

It was suggested that non-mammaliaform cynodonts may have evolved burrowing as a behavioural strategy (Damiani *et al.* 2003, Iqbal 2013) to escape the harsh environmental conditions (Bordy *et al.* 2009) that followed the Permian-Triassic mass extinction event 252 million years ago (MA). Accordingly, this mode of survival may have been instrumental to success of the lineage that gave rise to

mammals in the Jurassic (Ruta *et al.* 2013). Discovering a specimen inside a burrow is not necessarily indicative of the animal being fossorial, however, as animals can occupy burrows opportunistically, whether they have the ability to create their own burrow or not (Lamping 2012). Musculoskeletal structure convergent on that of known fossorial animals (e.g. wombats) would provide more definitive evidence for this type of adaptive behavioural strategy (and morphology) than would an association with a fossilized burrow cast. It is evident that the musculature of the forelimb plays an important role in the mode of behaviour of the organism (Abdala and Moro 2006). However, there has been a lack of internal (e.g., cross-sectional properties) skeletal description of *Thrinaxodon*'s forelimb. The forelimbs of fossorial species are stout and robust with large areas of muscle attachments (Milne *et al.* 2009; Elissamburu and De Santis 2011). In a recent morphological study using landmarks (Iqbal 2013, Iqbal *et al.* in prep), humeral shape of *Thrinaxodon* was morphologically closer to that of wombats, which is a well-known fossorial marsupial, than it was to that of *Varanus niloticus* and *Thylacinus cynocephalus*. This evidence supports the hypothesis of *Thrinaxodon* as a potential burrow maker (Iqbal 2013). However, intriguingly, the radius retained a form resembling the condition of digging reptiles, which also have a sprawled limb posture (Iqbal 2013).

In addition to selective pressures generated by fossorialism, morphology of *Thrinaxodon* forelimbs undoubtedly is shaped by selective pressures associated with gait type. Skeletal elements of the forelimb are likely adapted according to locomotion and habitual gait posture, as well as active fossorialism (Turnbull and Reed 1967; Szalay 1994; Iqbal 2013). A few morphological characteristics in the limb of *Thrinaxodon* are interpreted as to allow for larger muscle attachment (Kemp 2005), thus supporting the body off the ground (Kardong 2009). However, this degree of attachment decreased across cynodonts towards modern mammals, permitting the limbs to adopt a parasagittal posture (Blob 2001). Detailed quantitative studies of forelimb posture in therapsids, including *Thrinaxodon*, are lacking and this has resulted in an interpreted semi-sprawling posture for all non-mammaliaform therapsids (Jenkins 1971). In fact, transition from the sprawling posture of reptilian forelimbs to a more erect mammalian

parasagittal posture receives critical support in the semi-sprawled gait reconstruction attributed to *Thrinaxodon* (Reilly and Delancey 1997; Blob and Biewener 1999; Damiani *et al.* 2003; Iqbal 2013). A recent study (Iqbal 2013) demonstrated structural trends in broad humeral epiphyses that provide large areas for muscle attachment in the forelimb of *Thrinaxodon*, noting that they fall between those of the mammalian wombat and the reptilian *Varanus* forelimb which suggested a mosaic pattern of features indicating digging ability and sprawled limb posture.

In order to evaluate the evolutionary origins of forelimb functional morphology in *Thrinaxodon* *liorhinus*, comparison with a non-burrowing cynodont relative, *Cynognathus*, and a dicynodont, *Cistecephalus* that exhibits fossorial morphology in the forelimb, is necessary. *Cynognathus* was one of the larger carnivorous cynodonts common during the Early-Middle Triassic (Solomon *et al.* 2011). This species was estimated to be two metres in body length with the hind limbs directly underneath the body and the forelimbs semi-sprawled (Jenkins 1971; Palmer 1999; Nasterlack *et al.* 2013). *Cistecephalus*, a dicynodont from the Late Permian, is interpreted as a specialized burrower because of specialized features in its forelimbs resembling those of modern burrowing mammals (Cluver 1978; Palmer 1999).

Extant reptiles present a marked heterogeneity in terms of adaptive strategies (e.g., arboreal, rock-dwelling, fossorial), making them an ideal comparative group for providing insight into understanding form-function relationships in the limb musculoskeletal anatomy of the fossil species. There are different types of digging behavior (e.g., occasional digger, scratch digger, generalized digger, etc.) that digging reptiles, as well as other fossorial animals, exhibit. These may be reflected in minor differences of the limb bone morphology depending on how these types of digging behavior affect the bone structure.

Research on posture and behaviour in the cynodont, *Thrinaxodon*, has not fully determined functional morphology of the forelimb as reflecting adaptation to fossorialism or response to the semi-sprawling posture, nor have quantitative analyses (e.g., geometric morphometric approaches) been applied in addressing this issue. The main goal of this study is to enhance insight into the functional

morphology of the forelimb of *Thrinaxodon*, primarily through comparisons with those of a burrower mammal and a variety of reptiles with different general activity patterns. Forelimb structure is externally assessed using geometric morphometrics, a qualitative analysis of muscle attachment and internally assessed using cross-sectional geometric properties. This will allow for a comprehensive understanding of the overall variability in functional morphology of cynodont forelimbs, and specifically, a better understanding of which features drive observed morphological differences. Achieving these aims will allow specific hypotheses to be addressed.

1. The forelimb of the mammal-like cynodont *Thrinaxodon* is adapted for burrowing. If the fossil taxon resemble fossorial marsupials and reptiles, these features would seem to be related to fossorial behavior and relatively independent of phylogeny.
2. Alternatively, the forelimb musculoskeletal structure of *Thrinaxodon* may be adapted to semi-sprawled posture and gait. Where the fossil taxon (i.e., *Thrinaxodon*) resemble fossorial reptiles only, these features could resemble either gait type or fossorial behavior, unless resemblance with other reptiles (e.g., non-digging reptiles) was minimal.
3. The forelimb of *Thrinaxodon*, presumably adapted for digging, should exhibit greater configurational similarity to the forelimb of the dicynodont *Cistecephalus*, also regarded as a fossorial taxon, than *Cynognathus*, generally considered to be a non-fossorial cynodont.
4. The forelimb structure of the fossil taxa, *Cistecephalus* and *Cynognathus*, share similarities with *Thrinaxodon* that are not shared by modern taxa, indicating a phylogenetic signal.

Materials and Methods

Materials

Morphological features of the right forelimb of fossil taxa were included for *Thrinaxodon liorhinus* (BPI/1/7199), which was found in a burrow cast numbered BPI/1/ 5558; *Cynognathus* (BPI/1/1675) and *Cistecephalus* (BPI/1/2915); which is housed at the Evolutionary Studies Institute,

University of the Witwatersrand. Due to time constraints, only one specimen of *Thrinaxodon* was used. Fossil specimens were compared to forelimbs of extant reptilian species characterised by non-digging and digging behaviours in order to infer functional components of the exhibited morphology. Extant taxa included: arboreal reptiles – *Anolis equestris* (n = 2); non-digging reptiles – *Cordylus warreni* (n = 1), *Platysaurus imperator* (n = 1), *Pseudocordylus melanotus* (n = 2); digging reptiles – *Cordylus giganteus* (n = 3), *Crocodylus moreletti* (n = 1), *Crocodylus niloticus* (n = 1), *Crocodylus* sp. (n = 1), *Gerrhosaurus validus* (n = 1) and *Varanus niloticus* (n = 2) (Table 1). Extant marsupials, *Lasiorhinus krefftii* (n = 1) and *Vombatus ursinus* (n = 2), were used as phylogenetic outgroups for evaluation of structural and functional aspects of the forelimb associated with fossorialism (Table 1).

Table 1: Sample Composition

Category	Taxon	Specimen number	Common Name	Source*	Behavioural Category
Therapsid	<i>Thrinaxodon liorhinus</i>	BPI/1/7199		ESI	Fossorial
Therapsid	<i>Cynognathus</i>	BPI/1/1675		ESI	Non-fossorial
Therapsid	<i>Cistecephalus</i>	BPI/1/2915		ESI	Fossorial
Reptile	<i>Anolis equestris</i>	R59327	Cuban Knight Anoles	MCZ	Arboreal
Reptile	<i>Anolis equestris</i>	R59328	Cuban Knight Anoles	MCZ	Arboreal
Reptile	<i>Cordylus warreni</i>	R45805	Warren's Girdled Lizard	MCZ	Rock-dweller
Reptile	<i>Platysaurus imperator</i>	R67614	Emperor Flat Lizard	MCZ	Rock-dweller
Reptile	<i>Pseudocordylus melanotus</i>	R184420	Drakensberg Crag Lizard	MCZ	Rock-dweller
Reptile	<i>Pseudocordylus melanotus</i>	TMS 143	Drakensberg Crag Lizard	DNMNH	Rock-dweller
Reptile	<i>Cordylus giganteus</i>	R39384	Giant Girdled Lizard	MCZ	Fossorial
Reptile	<i>Cordylus giganteus</i>	TMS 133	Giant Girdled Lizard	DNMNH	Fossorial
Reptile	<i>Cordylus giganteus</i>	TMS 137	Giant Girdled Lizard	DNMNH	Fossorial
Reptile	<i>Crocodylus moreletti</i>	R8047	Morelet's Crocodile	MCZ	Fossorial
Reptile	<i>Crocodylus niloticus</i>	TMS 150	Nile Crocodile	DNMNH	Fossorial

Reptile	<i>Crocodylus</i> sp.	ZA913	Crocodile	SAS	Fossorial
Reptile**	<i>Crocodylus</i> sp.	Fresh Specimen	Crocodile	SAS	Fossorial
Reptile	<i>Gerrhosaurus validus</i>	R44579	Giant Plated Lizard	MCZ	Fossorial
Reptile	<i>Varanus niloticus</i>	VN1	Nile monitor	APES	Fossorial
Reptile	<i>Varanus niloticus</i>	VN2	Nile monitor	APES	Fossorial
Mammal	<i>Lasiorhinus kreffti</i>	J14051	Northern Hairy-nosed Wombat	TM	Fossorial
Mammal	<i>Vombatus ursinus</i>	M10000	Common Wombat	ANWC	Fossorial
Mammal	<i>Vombatus ursinus</i>	A1258	Common Wombat	QM	Fossorial

* ESI: Evolutionary Studies Institute at the University of the Witwatersrand (South Africa); APES: Animal, Plants and Environmental Sciences Museum at the University of the Witwatersrand (South Africa); SAS: School of Anatomical Sciences at the University of the Witwatersrand (South Africa); DNMMH: Ditsong National Museum of Natural History (South Africa); MCZ: Museum of Comparative Zoology at Harvard University (Massachusetts); ANWC: Australian National Wildlife Collection (Canberra); QM: Queensland Museum (Brisbane); TM: Tasmanian Museum (Hobart)

** The fresh specimen that was used for dissecting purposes was obtained from the School of Anatomical Sciences at the University of the Witwatersrand with the help of Prof. Paul Manger and Mr. Brendon Billings.

The forelimb of *Varanus niloticus* and that of *Vombatus ursinus* and *Lasiorhinus kreffti*, have been examined previously (Iqbal 2013; Iqbal *et al.* In prep), and were shown to be broadly comparable to that of *Thrinaxodon*. These four specimens allowed for a better understanding of the extent to which *Thrinaxodon* forelimb resembles either fossorial mammals or reptiles.

Gerrhosaurus sp. is fossorial, and is adapted to living on rocky out-crops (Branch 1998; Alexander and Marais 2007). *Cordylus giganteus* is a sunbathing lizard that lives in burrows (Branch 1998; Alexander and Marais 2007). *Crocodylus niloticus* is the second largest extant reptile, and is found throughout Sub-Saharan Africa (Branch 1998). Juveniles of this species often dig burrows to inhabit for up to four years (Branch 1998). They exhibit short but strong limbs (Alexander and Marais 2007). *Cordylus warreni* is one of the few non-digging reptiles in southern Africa (Branch 1998). They are found on mountainous slopes that are rocky with deep fractures that allow sheltering during hot-dry seasons

(Branch 1998; Alexander and Marais 2007). *Platysaurus imperators* are rock-dwelling, non-digging, savanna lizards (Branch 1998; Alexander and Marais 2007). *Pseudocordylus melanotus*, a non-digging reptile, is found in large colonies in rocky outcrops (Alexander and Marais 2007). *Anolis equestris* is native to Cuba and are strictly arboreal lizards (Nicholson and Richards 2011).

Methods

The forelimbs of *Cynognathus* BPI/1/1675, *Cistecephalus* BPI/1/2915, *Cordylus giganteus* (TMS 133 and TMS 137), *Crocodylus* ZA 913, *Crocodylus niloticus* TMS 150, *Pseudocordylus melanotus* TMS 143 and *Varanus niloticus* were scanned using high resolution computed tomography (CT). The Nikon Metrology XT H 225 LC microCT scanner located in the Evolutionary Studies Institute (ESI) at the University of the Witwatersrand (www.wits.ac.za/microCT) (see Table 2 for scan parameters) and the Skyscan 1173 microCT at the Museum of Comparative Zoology (www.mcz.harvard.edu) was used for acquiring data from the above-mentioned species (Table 2). Other material, such as the *Thrinaxodon liorhinus* specimen (BPI/1/ 7199), was scanned at the European Synchrotron Radiation Facility (ESRF, France, Grenoble) on ID 17 beamline using a monochromatic beam 96 keV, isotropic voxels of 45.5 microns, and 4000 projections (Fernandez *et al.* 2013; Iqbal *et al.* In prep). The marsupial specimens (*Lasiornhinus krefftii* J14051, *Vombatus ursinus* A1258 and M10000) were scanned with a medical CT scanner using different scan parameters: tube voltage = 120 kV; tube current = 200mA-300mA; slice thickness = 0.5-0.625 mm, reconstruction increment = 0.4 mm; 512x512 voxel matrix (Carlson *et al.* 2013).

Table 2: Scan parameters that used to CT-scan specimens at the ESI and MCZ

Species	Species number	Location	Tube voltage (kV)	Tube current (μ A)	Frames per second	Projections	Isotropic voxel size (micron)
<i>Cynognathus</i>	BPI1675	ESI	85	100	1	3600	57.3
<i>Cistecephalus</i>	BPI2915	ESI	110	155	1	4000	35.9
<i>Cordylus giganteus</i>	TMS133 and TMS137	ESI	50	195	1	2000	16.6
<i>Crocodylus</i>	ZA913	ESI	70	125	1	2000	84.3
<i>Crocodylus niloticus</i>	TMS150	ESI	50	195	1	2000	16.6
<i>Pseudocordylus melanotus</i>	TMS143	ESI	50	195	1	2000	16.6
<i>Varanus niloticus</i>	VN1 and VN2	ESI	75	115	1	360	50
<i>Crocodylus moreletti</i>	R8047	MCZ	130	61		2240	33.04
<i>Cordylus giganteus</i>	R39384	MCZ	130	61		2240	35.53
<i>Gerrhosaurus validus</i>	R44579	MCZ	130	61		2240	35.53
<i>Cordylus warreni</i>	R45805	MCZ	130	61		2240	31.97
<i>Platysaurus imperator</i>	R67614	MCZ	130	61		2240	35.17
<i>Pseudocordylus melanotus</i>	R184420	MCZ	130	61		2240	31.97

* *Anolis equestris*, R59327 and R59328, scan parameters were not given for this research and were scanned at the Museum of Comparative Zoology (MCZ) using a skyscan.

The 3D rendering of skeletal elements that were generated from the resultant image stacks were produced using VG Studio Max 2.1 (Volume Graphics, Heidelberg, Germany) and/or Avizo Standard 7.1.1 (VSG, Merignac, France). Segmenting and separating elements that remained in contact with other elements in image stacks was performed using Avizo 7.1.1. Shape analyses and quantifications of internal structure were performed using these programs, as well as other analytical software (example: ImageJ v1.48, Mophologica v2.5).

Using the digital calipers option in Avizo 7.1.1, seven linear measurements (Figure 1) were taken, from which five functional indices were calculated. These indices reflect mechanical usage of muscles related to humerus and ulna function (Elissamburu and Vizcaino 2004; Elissamburu and De Santis 2011):

- Shoulder moment index (SMI) – length of the deltoid insertion on the humerus (DLH) divided by the functional length of the humerus (HL).
- Humerus robustness index (HRI) – transverse diameter of the humerus midshaft (TDH) divided by the functional length of the humerus (HL).
- Epicondyle index (EI) – epicondylar width of the humerus (DEH) divided by the functional length of the humerus (HL).
- Index of fossorial ability (IFA) – proximo-distal length of the olecranon process (OL) divided by the functional ulna length (FUL).
- Ulna robustness index (URI) – transverse diameter of the ulna midshaft (TDU) divided by the functional ulna length (FUL).

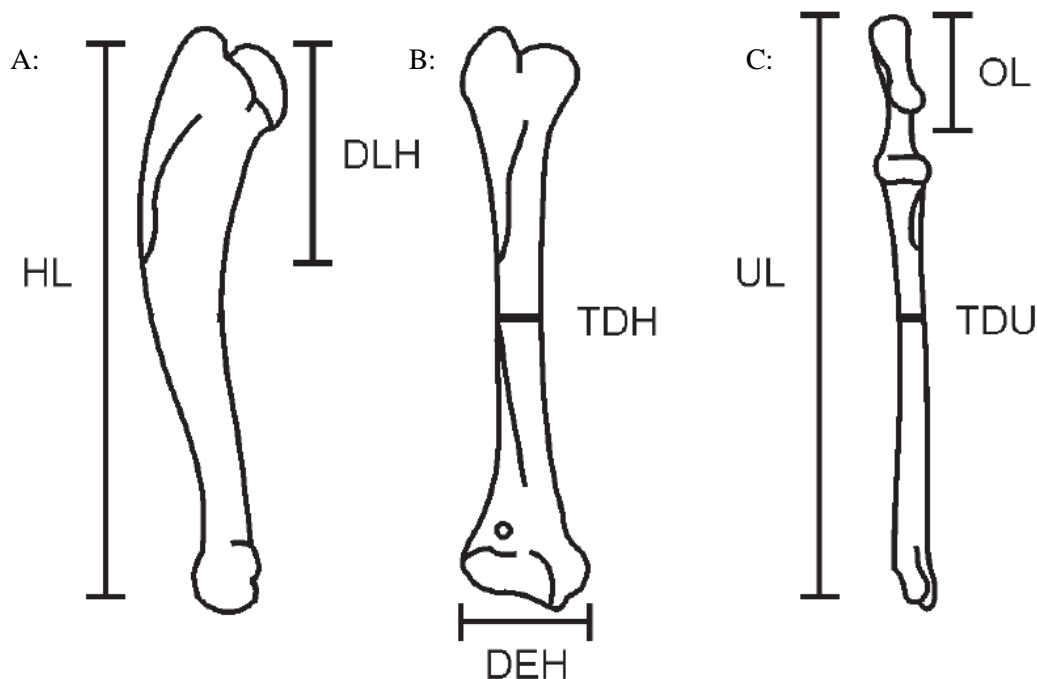


Figure 1: A, B: humerus; C: ulna. Measurements taken for the indices. DEH – diameter of the epicondyles; DLH – deltoid length of the humerus; HL – functional humerus length; OL – olecranon length from the tip of the olecranon process to the centre of the trochlear notch; TDH – transverse diameter of the humerus at the midpoint; TDU – transverse diameter of the ulna at the

midpoint; UL – functional ulna length (Figure adapted from Elissamburu and Vizcaino 2004; Elissamburu and De Santis 2011).

Cortical thickness was analysed only for humeri as the internal properties proved to be challenging to quantify during the segmentation process. It was not always possible to reliably discern medullary cavities in the ulna and radius. The images were taken in Avizo 7.1.1 where the humeral bone was aligned so that the frontal, longitudinal and transverse planes were centred before taking snapshots of midshaft cross-sections (50% of full length). The scale for images was analysed on ImageJ, and then imported into Scion Image (release Beta 4.0.2). Resultant images were analysed using custom-written macros (Carlson 2005). Briefly, this involved inverting images and establishing an upper and lower threshold range that highlighted the cortical bone in the cross section. Subsequently, cortical bone was selected in order to calculate cross-sectional properties. Standard cross-sectional properties were acquired: Periosteal Area (Ps.Ar), Cortical Area (Ct.Ar), second moments of area about anteroposterior (AP) (I_y) and mediolateral (ML) (I_x), principal moments of area (I_{max} , I_{min}) and the principal angle (Θ) (Carlson 2014). Percentage cortical area (% Ct.Ar) was computed as Ct.Ar. divided by Ps.Ar, and multiplied by 100. The polar moment of area (J), was calculated as the sum of I_{max} and I_{min} . J quantifies resistance to torsion whereas the average bending rigidity (J/2) represents a measure of overall bending rigidity of the diaphysis. Cross-sectional properties (I_y , I_x , I_{max} , I_{min} and J) were standardised by natural logging the variable divided by the length of the humerus to the fourth power, i.e., $[\ln(\text{variable}/\text{length})^4]$. Standardising cross-sectional properties is customary, as these are known to exhibit allometric relationships with body size. Cross-sectional properties determines stress and displacement of a bone that undergoes bending and torsional loads (O'Neill and Ruff 2004; Lieberman *et al.* 2004; Ruff and Larson 2014).

Each rendered element was aligned to a common morphospace and then standardized (equalised in length) to the length of respective elements of a representative *Vombatus ursinus* (M10000) (Table 3). This permitted exclusively analysing shape changes of the proximal and distal ends as well as torsion

amongst the elements. By standardizing bones to equal lengths, direct effects of allometry were reduced.

The purpose of the analysis was to assess configurational differences rather than size differences.

Geometric morphometric (GM) landmark-based analyses were used to measure morphological similarities between each element of the forelimb elements (humerus, radius and ulna) in order to assess functional similarities. Landmarks were placed on analogous structures of rendered elements using Avizo

7.1.1. The chosen landmarks emphasize articular surfaces and muscle attachment areas (Milne *et al.* 2009). A combined total of 70 landmarks were chosen on the forelimb skeleton: twenty-nine humeral (Table A3), eighteen radial (Table A4) and twenty-three ulnar (Table A5) (Iqbal 2013; Iqbal *et al.* In prep).

Table 3: The scale factor that was used to standardize the elements to the length of *Vombatus ursinus* M10000.

	Humeri	Radii	Ulnae
<i>Vombatus ursinus</i> M10000	To 117.73 mm	To 104.55 mm	To 136.03 mm
<i>Vombatus ursinus</i> A1258	Scaled by: 1.171	Scaled by: 0.91	Scaled by: 1.115
<i>Lasiorhinus krefftii</i> J14051	Scaled by: 1.025	Scaled by: 0.92	Scaled by: 0.99
<i>Thrinaxodon liorhinus</i> BPI5558	Scaled by: 3.675	Scaled by: 3.69	Scaled by: 4.68
<i>Cynognathus</i> BPI 1675 (large)*	Scaled by: 1.25	Scaled by: 0.95	Scaled by: 0.99
<i>Cynognathus</i> BPI 1675 (small)*		Scaled by: 1.2	Scaled by: 1.7
<i>Cistecephalus</i> BPI2915	Scaled by: 3.7	Scaled by: 5	Scaled by: 5
<i>Anolis equestris</i> R59327	Scaled by: 15	Scaled by: 18	Scaled by: 23
<i>Anolis equestris</i> R59328	Scaled by: 16	Scaled by: 19	Scaled by: 23
<i>Cordylus warreni</i> R45805	Scaled by: 6.5	Scaled by: 9	Scaled by: 11
<i>Platysaurus imperator</i> R67614	Scaled by: 5	Scaled by: 7	Scaled by: 9
<i>Pseudocordylus melanotus</i> R184420	Scaled by: 9	Scaled by: 13	Scaled by: 15
<i>Pseudocordylus melanotus</i> TMS143	Scaled by: 8	Scaled by: 10	Scaled by: 12
<i>Cordylus giganteus</i> R39384	Scaled by: 5	Scaled by: 7	Scaled by: 7
<i>Cordylus giganteus</i> TMS133	Scaled by: 4	Scaled by: 5	Scaled by: 6
<i>Cordylus giganteus</i> TMS137	Scaled by: 5	Scaled by: 6.5	Scaled by: 8

<i>Crocodylus moreletti</i> R8047	Scaled by: 5	Scaled by: 7	Scaled by: 8
<i>Crocodylus niloticus</i> TMS150	Scaled by: 6	Scaled by: 8	Scaled by: 9
<i>Crocodylus</i> ZA913	Scaled by: 0.75	Scaled by: 1.2	Scaled by: 1.4
<i>Gerrhosaurus validus</i> R44579	Scaled by: 11	Scaled by: 13	Scaled by: 16
<i>Varanus niloticus</i> VN1	Scaled by: 2.315	Scaled by: 2.88	Scaled by: 3.25
<i>Varanus niloticus</i> VN2	Scaled by: 2.2735	Scaled by: 2.72	Scaled by: 3

* Two different sized radius and ulna of *Cynognathus* was used for analyses.

Torsion is the twist of the longitudinal shaft of one end of the bone (proximal) relative to the other end (distal) due to a strain acting upon the bone (Shah *et al.* 2006). Humeral torsion has been attributed to fossorial behavior and is linked to the expansion of muscle attachment area (Meier *et al.* 2013), however this does not characterised solely fossorial taxa (Evans 1978). Humeral torsion was calculated using the cross-product (vector product) of two vectors characterizing the proximal and distal ends of humeral shaft (Jashashvili *et al.* 2011). The torsion angle was computed as the inverse cosine of the product of two vectors, multiplied by 180 and then divided by pi ($\pi = 3.141592$), i.e., $[(\text{Acos}(\text{product of vectors}) * 180) / 3.141592]$.

MorphoTools 1.1 (Specht *et al.* 2007; Swiss NFS projects N° 205321-102024/1 and 205320-109303/1; Lebrun 2008; Lebrun *et al.* 2010) was used to apply GM analyses on the landmark 3D coordinates. First, a sample scheme was applied where each .stl and .ver files was specified so that MorphoTools would recognise the landmark data. This was followed by conducting principal component analyses (PCA) on the landmarks in order to assess configurational variation in the sample. MorphoTools allows the landmarks to be altered in a common morphospace essentially by deforming the original rendering along each principal component (Zelditch *et al.* 2004; Iqbal *et al.* In prep). In order to visualise variability of landmark configuration in morphospace, each principal component (PC) was plotted and deformed renderings at regular intervals were produced. The PC scores were analysed to illustrate configurational relationships between elements using JMP 11 (SAS, SAS Institute Inc., 2014). Lastly, a

regression was performed in order to explain the predictive relationship of the variables to one another. Logged centroid size was used as the independent variable in all regressions since it provides a useful approximation of overall size and is independent of shape. When a PC of interest is not correlated with logged centroid size, it reflects variance in the sample predominantly due to shape. For all statistical testing in the study, statistical significance was achieved when $p < 0.05$.

Muscle attachment sites

Muscle attachment scars on original fossils (or renderings of fossils) were used to define, when discernible, the extent of muscle attachment sites (Figure A7-A10). In some cases, this was not possible. As an alternative, the right forelimb of a single fresh specimen, *Crocodylus*, from the School of Anatomical Sciences at the University of the Witwatersrand was dissected and examined in order to infer origin and insertion sites of muscle attachments in the fossil taxa under investigation. It is understood that the musculoskeletal anatomy of *Crocodylus* may not entirely be suitable for representing the musculoskeletal anatomy of the fossil taxa, but it provided a basis for inference when none was possible otherwise.

Results

Geometric morphometric landmark-based analyses

Principal component analyses (PCAs) of landmark configurations were performed on the standardized forelimb, where the F-ratio was the sum of squares reflecting different sources of variability. For the humeri, PC1 (52.03%), PC2 (21.40%) and PC 3 (8.70%) explain most of the variation in the sample where PC1 (Figure 2) corresponds to shape ($r^2 = 0.00$, F-ratio = 0.05, $p > 0.82$) (Table 4, Figure A1) and PC2 (Figure 4) corresponds to width size ($r^2 = 0.15$, F-ratio = 3.29, $p > 0.09$) (Table 4, Figure A2). The correspondence of PC1 to shape and PC2 to size is evident in the warp factor when the slider is moved along respective PC axes and the wireframes/renderings are deformed accordingly. PC1 (37.92%,

$r^2 = 0.09$, F-ratio = 2.06, $p > 0.17$) and PC2 (23.70%, $r^2 = 0.00$, F-ratio = 0.00, $p > 0.98$) explain the most variation in radial configurations while PC3 accounts for 13.10% (Figure 6, Figure 8). PC1 (48.38%, $r^2 = 0.30$, F-ratio = 8.40, $p < 0.01$), PC2 (23.51%, $r^2 = 0.00$, F-ratio = 0.00, $p > 0.98$) and PC 3 (9.35%) accounts for the variation in the ulnae (Figure 10, Figure 12).

Humerus

Plotting PC1 vs. PC2 for humeri, illustrates no overlap along PC1 for *Thrinaxodon*, however, it lies on the axis that separates *Cynoganthus* and *Varanus* (digging reptile) from the fossorial mammals (Figure 2), i.e., *Thrinaxodon* is closest to fossorial mammals. The digging and non-digging reptiles overlap across PC1 (Figure 2). *Cistecephalus* overlaps with non-digging reptiles and digging reptiles along PC1 (Figure 2). *Cynognathus* is found to have the lowest PC1 score and the arboreal reptiles have the highest PC1 score (Figure 2). *Cynognathus* overlaps with the non-digging reptile, *Pseudocordylus melanotus* along PC2 (Figure 2, Figure 4). The arboreal reptiles, *Anolis equestris*, overlap along PC2 with fossorial mammals (Figure 2). A non-digging reptile, *Cordylus warreni*, overlaps with a digging reptile, *Cordylus giganteus*, along PC1 and PC2 (Figure 2).

Cistecephalus shows no overlaps along PC2 and PC3 (Figure 4). *Thrinaxodon* overlaps with the digging reptile, *Varanus*, along PC3 (Figure 4). There is no clear differentiation among the behavioural groups as each quadrant has digging and non-digging species (Figure 2, Figure 4). Figure 3 illustrates PC1 and Figure 5 PC2 for humeral displacement of the species under investigation with a humeral rendering in anterior view. The series of renderings visualise reduction of the deltopectoral crest, as well as decreased width at the proximal and distal ends.

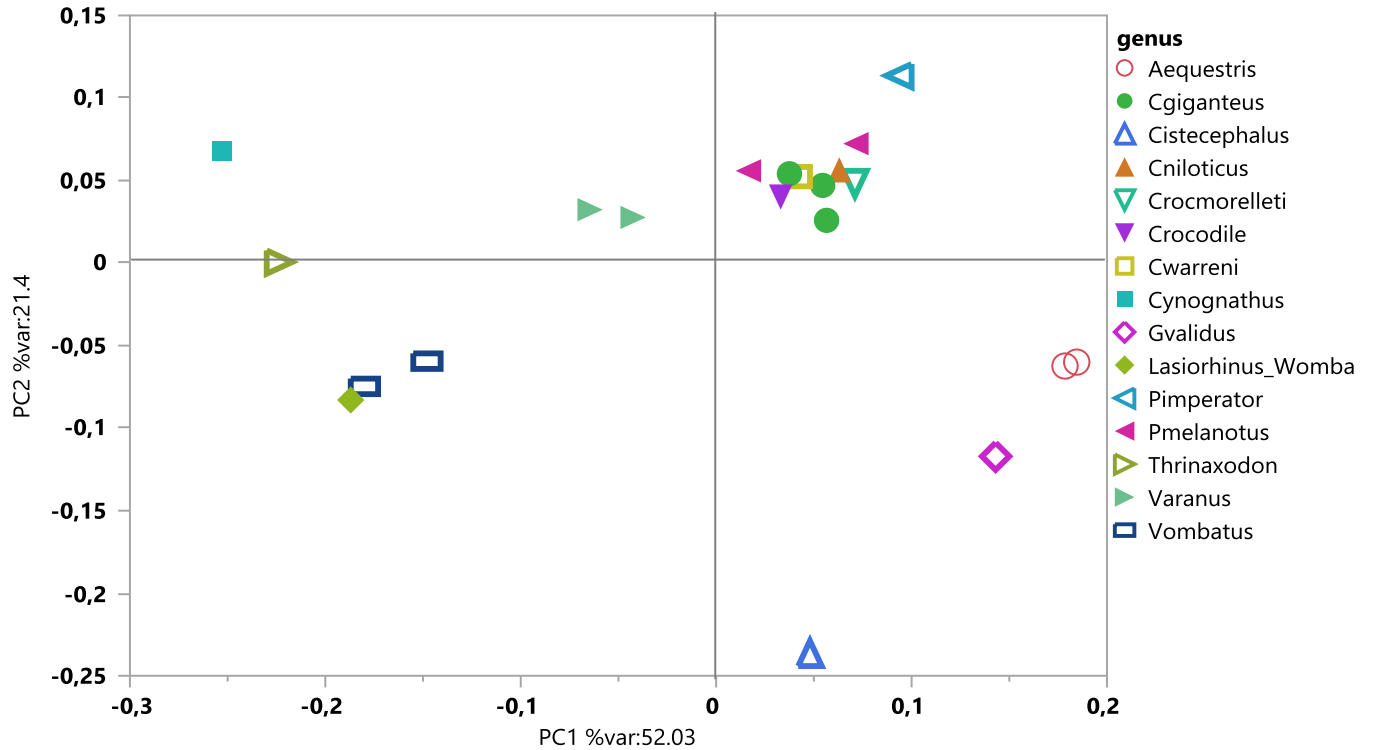


Figure 2: Plot of PC1 (x-axis) vs. PC2 (y-axis) for humeri. Aequestrtris: *Anolis equestris*, arboreal reptile. Cgiganteus: *Cordylus giganteus*, digging reptile. Cistecephalus, fossil. Cniloticus: *Crocodylus niloticus*, digging reptile. Crocmorelleti: *Crocodylus moreletti*, digging reptile. Crocodile, digging reptile. Cwarreni: *Cordylus warreni*, non-digging reptile. Cynognathus, fossil. Gvalidus: *Gerrhosaurus validus*, digging reptile. Lasiorhinus_Wombat: *Lasiorhinus krefftii*, fossorial mammal. Pimperator: *Platysaurus imperator*, non-digging reptile. Pmelanotus: *Pseudocordylus melanotus*, non-digging reptile. Thrinaxodon: *Thrinaxodon liorhinus*, fossil. Varanus: *Varanus niloticus*, digging reptile. Vombatus: *Vombatus ursinus*, fossorial mammal.

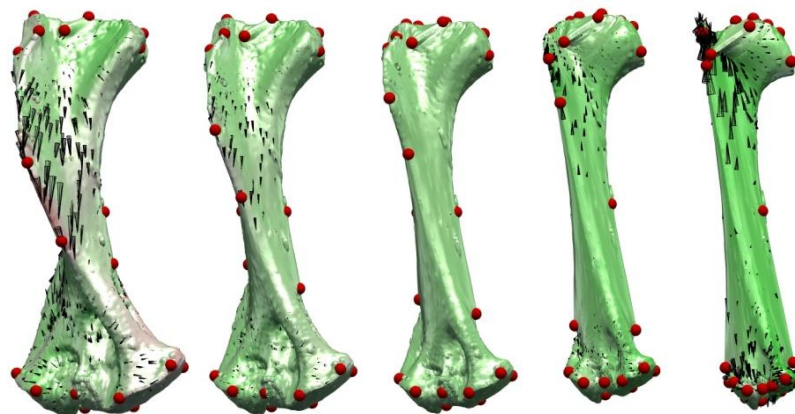


Figure 3: Anterior displacement of the humeral PC1 – to PC1 + from -0.2, -0.1, 0, 0.1, 0.2 respectively.

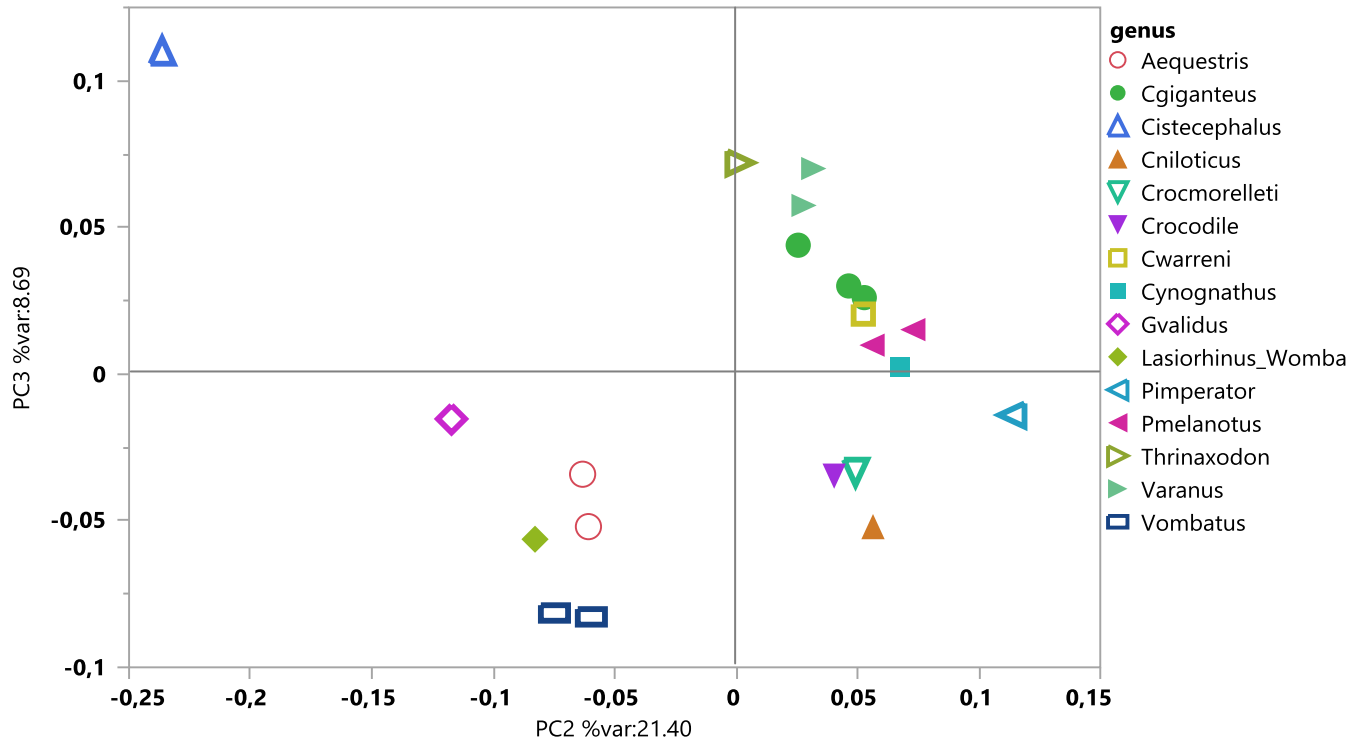


Figure 4: Plot of PC2 (x-axis) vs. PC3 (y-axis) for humeri. Aequestris: *Anolis equestris*, arboreal reptile. Cgiganteus: *Cordylus giganteus*, digging reptile. Cistecephalus, fossil. Cniloticus: *Crocodylus niloticus*, digging reptile. Crocmorelleti: *Crocodylus moreletti*, digging reptile. Crocodile, digging reptile. Cwarreni: *Cordylus warreni*, non-digging reptile. Cynognathus, fossil. Gvalidus: *Gerrhosaurus validus*, digging reptile. Lasiorhinus_Wombat: *Lasiorhinus krefftii*, fossorial mammal. Pimperator: *Platysaurus imperator*, non-digging reptile. Pmelanotus: *Pseudocordylus melanotus*, non-digging reptile. Thrinaxodon: *Thrinaxodon liorhinus*, fossil. Varanus: *Varanus niloticus*, digging reptile. Vombatus: *Vombatus ursinus*, fossorial mammal.

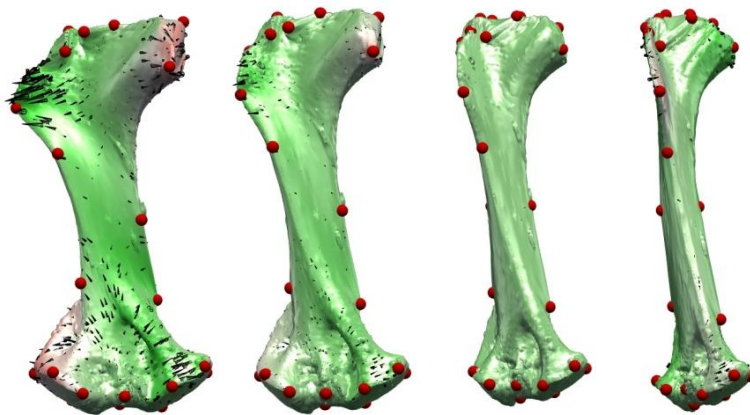


Figure 5: Anterior displacement of the humeral PC2 – to PC2 + from -0.2, -0.1, 0, 0.1 respectively.

Radius

Thrinaxodon does not overlap with any species along PC1 and PC2 (Figure 6). However, it shares the same quadrant as *Cynognathus*, *Cistecephalus* and *Crocodylus*, i.e., the therapsid fossil taxa are grouped together in relation to the extant species (Figure 6). No overlap occurs for *Cistecephalus* along PC1 (Figure 6), however, does overlap with digging reptiles along PC2 (Figure 8). The fossorial mammals overlap with digging reptiles, *Cordylus giganteus*, *Gerrhosaurus validus* and *Crocodylus niloticus* along PC1 for the radii (Figure 6). The arboreal species overlap with non-digging and digging reptiles along PC1 and PC2 (Figure 6). *Cynognathus* overlaps with digging and non-digging reptiles along PC2 (Figure 6).

Thrinaxodon does not overlap with any species, but lies closest to the extant reptiles in the positive axes (Figure 8). The fossorial mammals overlap with *Cynognathus* and the digging reptiles, *Cordylus giganteus* and *Crocodylus*, along PC3 (Figure 8). There is differentiation amongst the fossorial mammals and the extant reptiles (Figure 6, Figure 8). Figure 7 illustrates PC1 and Figure 9 PC2 radial displacement of the species under investigation with a posterior view, explaining a decrease in width of the overall radial bone.

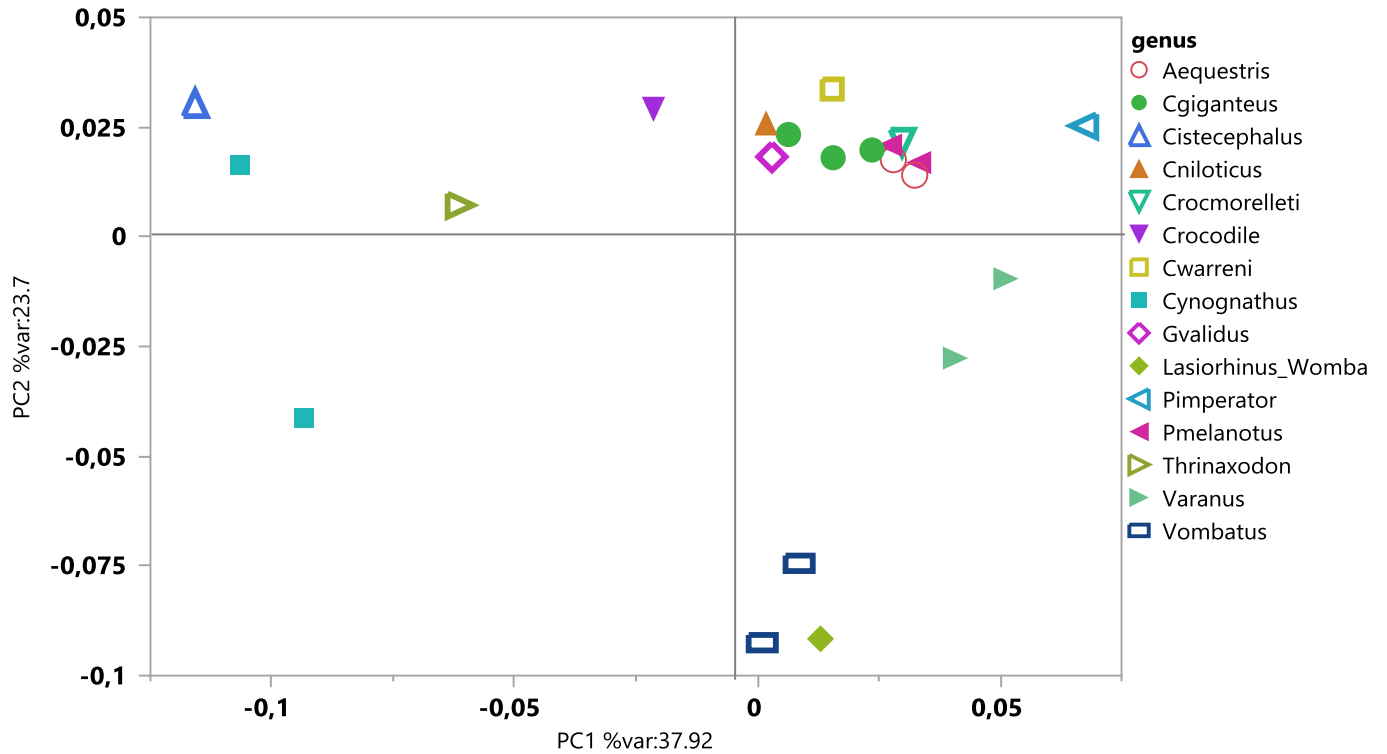


Figure 6: Plot of PC1 (x-axis) vs. PC2 (y-axis) for radii. Aequestrus: *Anolis equestris*, arboreal reptile. Cgiganteus: *Cordylus giganteus*, digging reptile. Cistecephalus, fossil. Cniloticus: *Crocodylus niloticus*, digging reptile. Crocmorelleti: *Crocodylus moreletti*, digging reptile. Crocodile, digging reptile. Cwarreni: *Cordylus warreni*, non-digging reptile. Cynognathus, fossil. Gvalidus: *Gerrhosaurus validus*, digging reptile. Lasiorhinus_Wombat: *Lasiorhinus kreffti*, fossorial mammal. Pimperator: *Platysaurus imperator*, non-digging reptile. Pmelanotus: *Pseudocordylus melanotus*, non-digging reptile. Thrinaxodon: *Thrinaxodon liorhinus*, fossil. Varanus: *Varanus niloticus*, digging reptile. Vombatus: *Vombatus ursinus*, fossorial mammal.

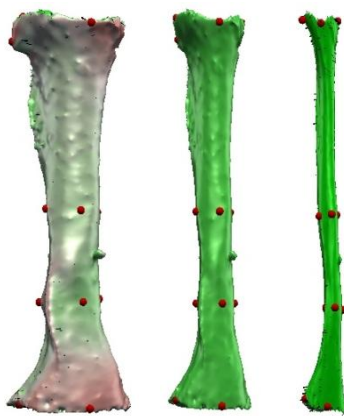


Figure 7: Posterior displacement of the radial PC1 – to PC1 + from -0.1, 0, 0.1 respectively.

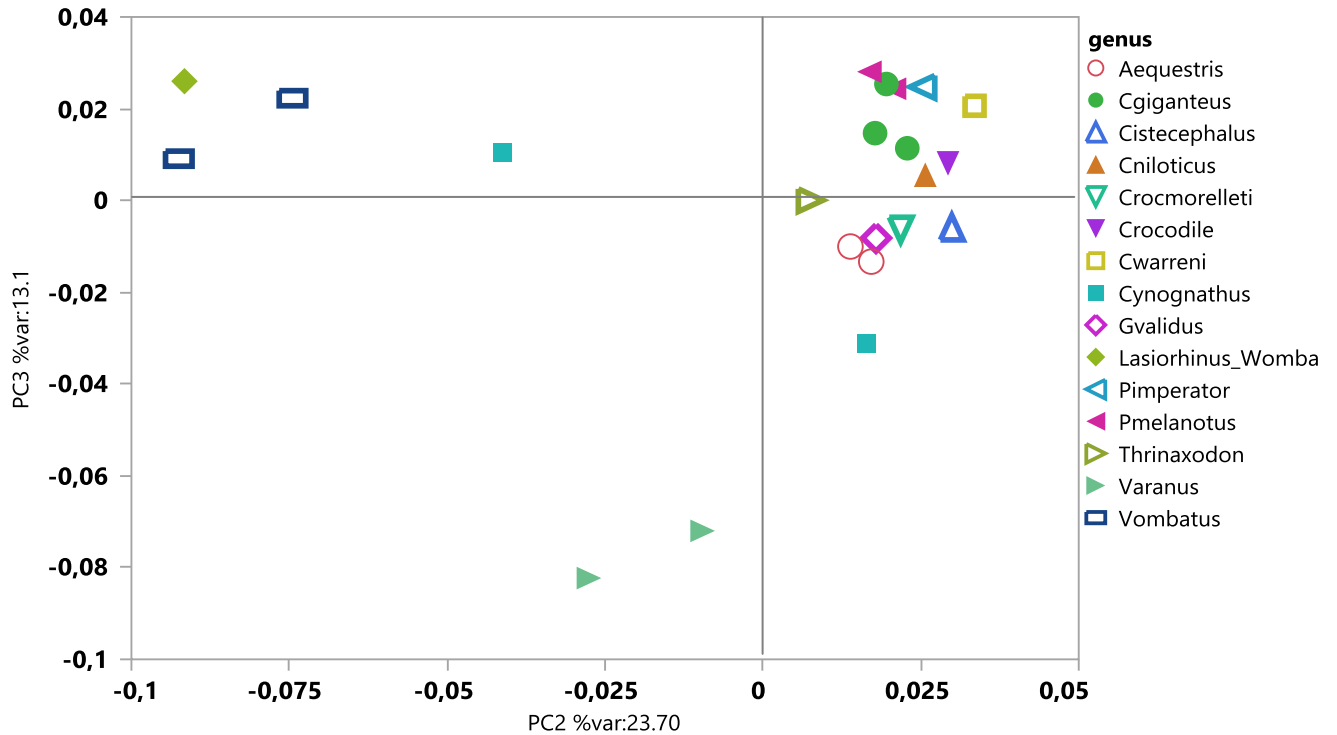


Figure 8: Plot of PC2 (x-axis) vs. PC3 (y-axis) for radii. Aequestrtris: *Anolis equestris*, arboreal reptile.

Cgiganteus: *Cordylus giganteus*, digging reptile. Cistecephalus, fossil. Cniloticus: *Crocodylus niloticus*, digging reptile. Crocmorelleti: *Crocodylus moreletti*, digging reptile. Crocodile, digging reptile. Cwarreni: *Cordylus warreni*, non-digging reptile. Cynognathus, fossil. Gvalidus: *Gerrhosaurus validus*, digging reptile. Lasiorhinus_Wombat: *Lasiorhinus krefftii*, fossorial mammal. Pimperator: *Platysaurus imperator*, non-digging reptile. Pmelanotus: *Pseudocordylus melanotus*, non-digging reptile. Thrinaxodon: *Thrinaxodon liorhinus*, fossil. Varanus: *Varanus niloticus*, digging reptile. Vombatus: *Vombatus ursinus*, fossorial mammal.



Figure 9: Posterior displacement of the radial PC2 – to PC2 + from -0.1, 0, 0.1 respectively.

Ulna

Thrinaxodon overlaps with non-digging reptiles, *Cordylus warreni* and *Pseudocordylus melanotus* (specimen R184420) along PC1 (Figure 10). The fossorial mammals do not overlap with any species along PC1 (Figure 10). It is worth noting that the fossorial mammals are the only species to exhibit an olecranon process on the ulna. *Cynognathus* (small) and the digging reptile, *Crocodylus moreletti* R8047 overlap along PC1, and *Cynognathus* (large) overlap with the digging reptiles, *Cordylus giganteus* (specimen TMS133) and *Crocodylus*, along PC1 (Figure 10). A non-digging reptile, *Platysaurus imperator*, overlaps with a digging reptile, *Crocodylus niloticus* (specimen TMS150), along PC1 (Figure 10). *Cistecephalus* overlap with digging reptiles along PC1 (Figure 10). *Varanus niloticus* (specimen VN1) overlaps with *Vombatus ursinus* (specimen A1258) along PC2 (Figure 10, Figure 12). This illustrates overlap amongst digging reptiles and fossorial mammals. There is minimal overlap along PC2 between *Cistecephalus* and *Cynognathus* (small) (Figure 10).

Thrinaxodon overlaps with the fossorial mammal, *Lasiorhinus krefftii*, along PC2 (Figure 12). It may be noted, that the therapsid fossils separate from extant species along PC2 (Figure 12). *Gerrhosaurus validus* and *Lasiorhinus krefftii* overlap along PC2 (Figure 10, Figure 12). Explaining overlap does occur between digging reptiles and fossorial mammals. The arboreal reptiles overlap with digging and non-digging reptiles along PC2 (Figure 12). There is overlap along PC3 between arboreal reptiles and fossorial mammals (Figure 12). In figure 10, there is clear separation amongst the fossorial mammals with the therapsid fossils and the extant reptiles. However, figure 12 illustrates separation amongst the therapsids fossils and the extant species, where the fossorial mammals overlap with the extant reptiles. Figure 11 illustrates PC1 ulnae displacement of the species under investigation with a lateral view, explaining the reduction of the proximal end and a decrease in width along the entire shaft for PC2 (Figure 13).

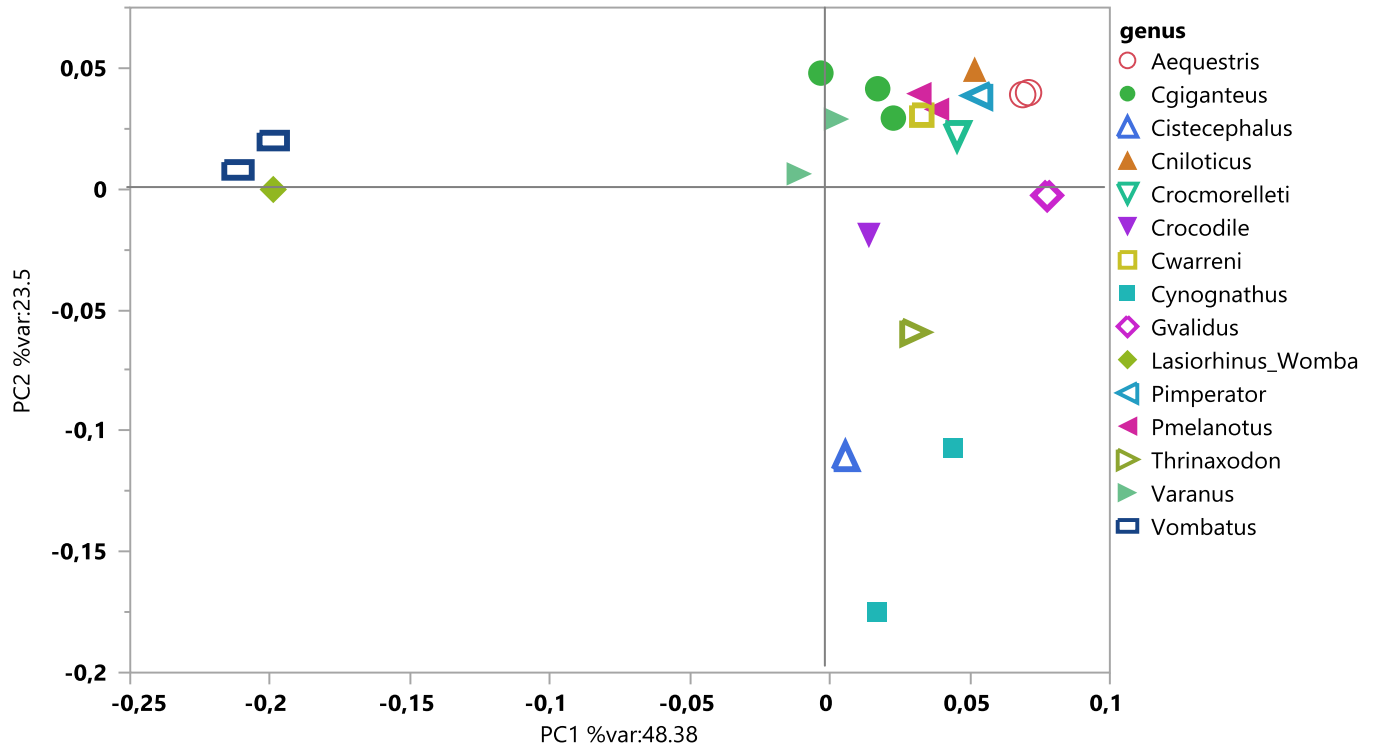


Figure 10: Plot of PC1 (x-axis) vs. PC2 (y-axis) for ulnae. Aequestrtris: *Anolis equestris*, arboreal reptile. Cgiganteus: *Cordylus giganteus*, digging reptile. Cistecephalus, fossil. Cniloticus: *Crocodylus niloticus*, digging reptile. Crocmoreletti: *Crocodylus moreletti*, digging reptile. Crocodile, digging reptile. Cwarreni: *Cordylus warreni*, non-digging reptile. Cynognathus, fossil. Gvalidus: *Gerrhosaurus validus*, digging reptile. Lasiorhinus_Wombat: *Lasiorhinus krefftii*, fossorial mammal. Pimperator: *Platysaurus imperator*, non-digging reptile. Pmelanotus: *Pseudocordylus melanotus*, non-digging reptile. Thrinaxodon: *Thrinaxodon liorhinus*, fossil. Varanus: *Varanus niloticus*, digging reptile. Vombatus: *Vombatus ursinus*, fossorial mammal.

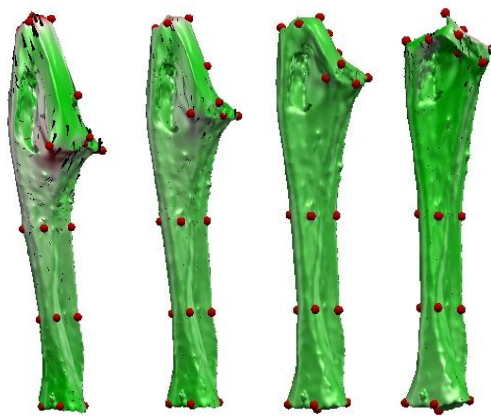


Figure 11: Lateral displacement of the ulnae PC1 – to PC1 + from -0.2, -0.1, 0, 0.1 respectively.

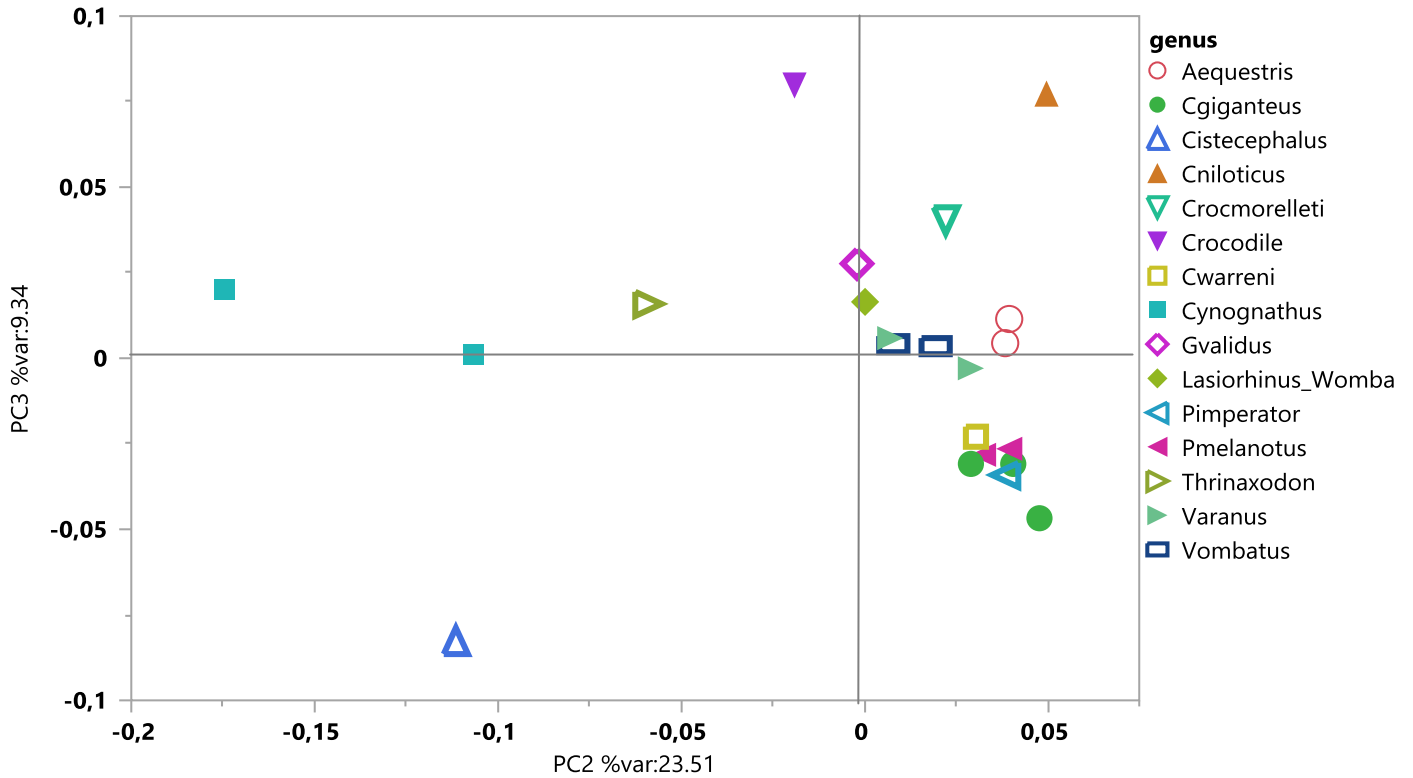


Figure 12: Plot of PC2 (x-axis) vs. PC3 (y-axis) for ulnae. Aequestrtris: *Anolis equestris*, arboreal reptile. Cgiganteus: *Cordylus giganteus*, digging reptile. Cistecephalus, fossil. Cniloticus: *Crocodylus niloticus*, digging reptile. Crocmoreletti: *Crocodylus moreletti*, digging reptile. Crocodile, digging reptile. Cwarreni: *Cordylus warreni*, non-digging reptile. Cynognathus, fossil. Gvalidus: *Gerrhosaurus validus*, digging reptile. Lasiorhinus_Wombat: *Lasiorhinus kreffti*, fossorial mammal. Pimperator: *Platysaurus imperator*, non-digging reptile. Pmelanotus: *Pseudocordylus melanotus*, non-digging reptile. Thrinaxodon: *Thrinaxodon liorhinus*, fossil. Varanus: *Varanus niloticus*, digging reptile. Vombatus: *Vombatus ursinus*, fossorial mammal.

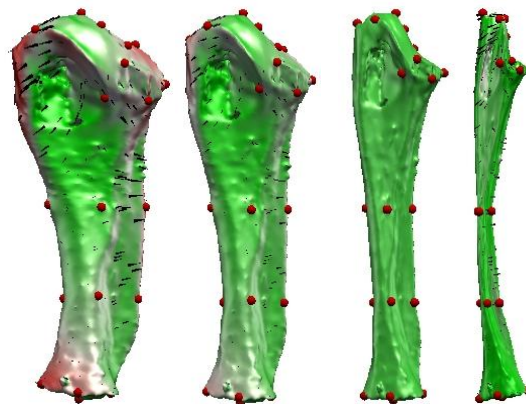


Figure 13: Lateral displacement of the ulnae PC2 – to PC2 + from -0.17, -0.1, 0, 0.1 respectively.

Table 4: Regression of the PC for the humeri, radii and ulnae vs. In Centroid Size

Humerus	R-squared	D.F	Sum of Squares	Mean Square	F Ratio	Prob > F
PC1 model	0,003	1	0,001	0,001	0,050	0,825
PC1 error		19	0,331	0,174		
PC2 model	0,148	1	0,020	0,202	3,292	0,085
PC2 error		19	0,117	0,006		
Radius	R-squared	D.F	Sum of Squares	Mean Square	F Ratio	Prob > F
PC1 model	0,094	1	0,005	0,005	2,063	0,166
PC1 error		20	0,048	0,002		
PC2 model	0	1	0	0	0	0,985
PC2 error		20	0,033	0,002		
Ulna	R-squared	D.F	Sum of Squares	Mean Square	F Ratio	Prob > F
PC1 model	0,296	1	0,046	0,046	8,398	0,009
PC1 error		20	0,109	0,005		
PC2 model	0	1	0	0	0,001	0,979
PC2 error		20	0,075	0,004		

Indices

1) *Shoulder Moment Index (SMI)*

Thrinaxodon has a SMI of 54.80%, which represents an average efficiency (Figure 14, Table A1). *Lasiorhinus krefftii* has the highest SMI with a 61.26% mechanical advantage (Table A1). Arboreal reptiles have the lowest SMI (Figure 14) with the *Anolis equestris* (specimen R59328) having a mechanical advantage of 9.84% (Table A1). Amongst extant comparative taxa, the SMI of non-digging reptiles ranges from 21.21% to 23.99%, while the SMI of digging reptiles ranges from 16.34% to 39.43% and that of fossorial mammals ranges from 60.12% to 61.26% (Figure 14, Table A1). The fossorial mammals, and *Cynognathus* and *Thrinaxodon* are the only species with over 50% mechanical advantage (Figure 14, Table A1).

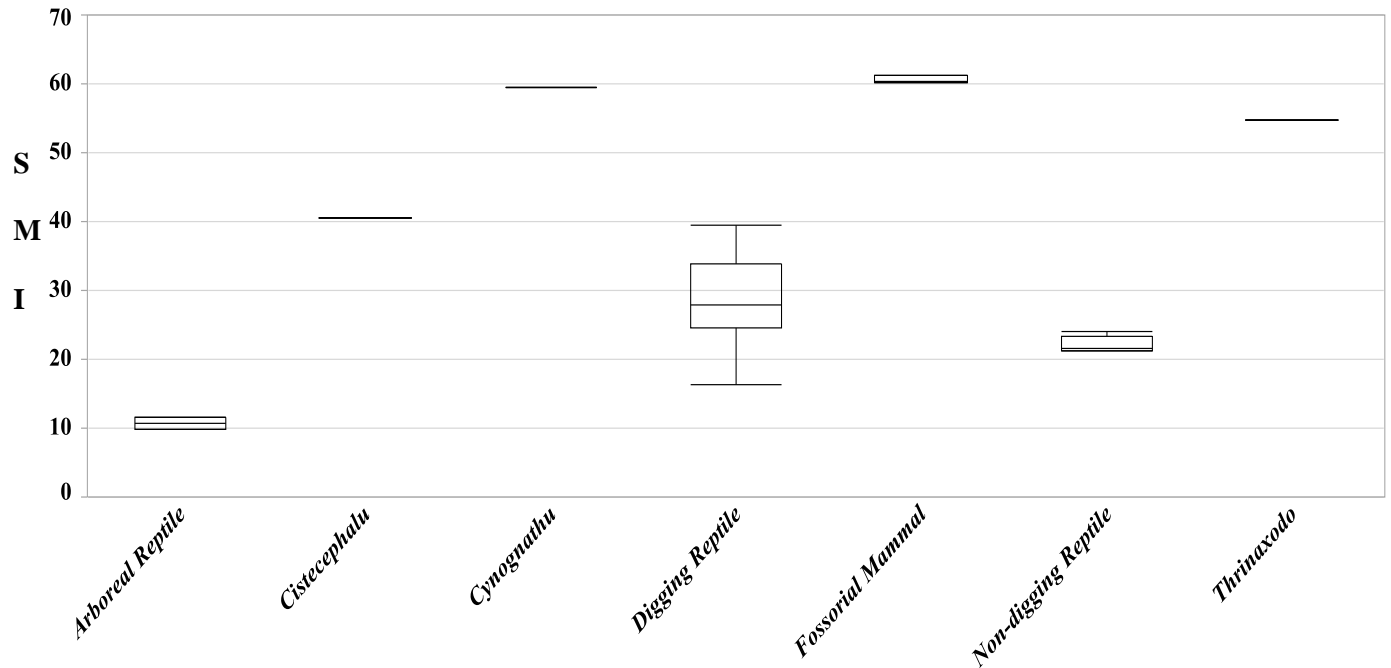


Figure 14: Box plot of the Shoulder Moment Index (SMI) for therapsid fossils, fossorial mammals and reptiles with different locomotor adaptations.

2) Humerus Robustness Index (HRI)

Thrinaxodon has a HRI of 15.33%, which is the third highest in the sample behind *Lasiorhinus kreffii* (specimen J14051) at 17.42% and *Vombatus ursinus* (specimen A1258) at 16.48% (Figure 15, Table A1). The arboreal reptiles, *Anolis equestris*, have the lowest HRI, 7.38% and 7.92% (Figure 15, Table A1). *Cynognathus* and *Cistecephalus* have HRI's of 13.16% and 14.61%, respectively (Figure 15, Table A1). From the digging reptile group, *Crocodylus* (specimen ZA913) has the highest HRI of 12.37% and *Varanus niloticus* (specimen VN1) has the second highest HRI of 11.81%, while the other digging reptiles are lower in HRI's, ranging around 9.0% HRI (Table A1). The non-digging reptiles have even lower HRI's ranging between 7.86% and 8.83% (Figure 15).

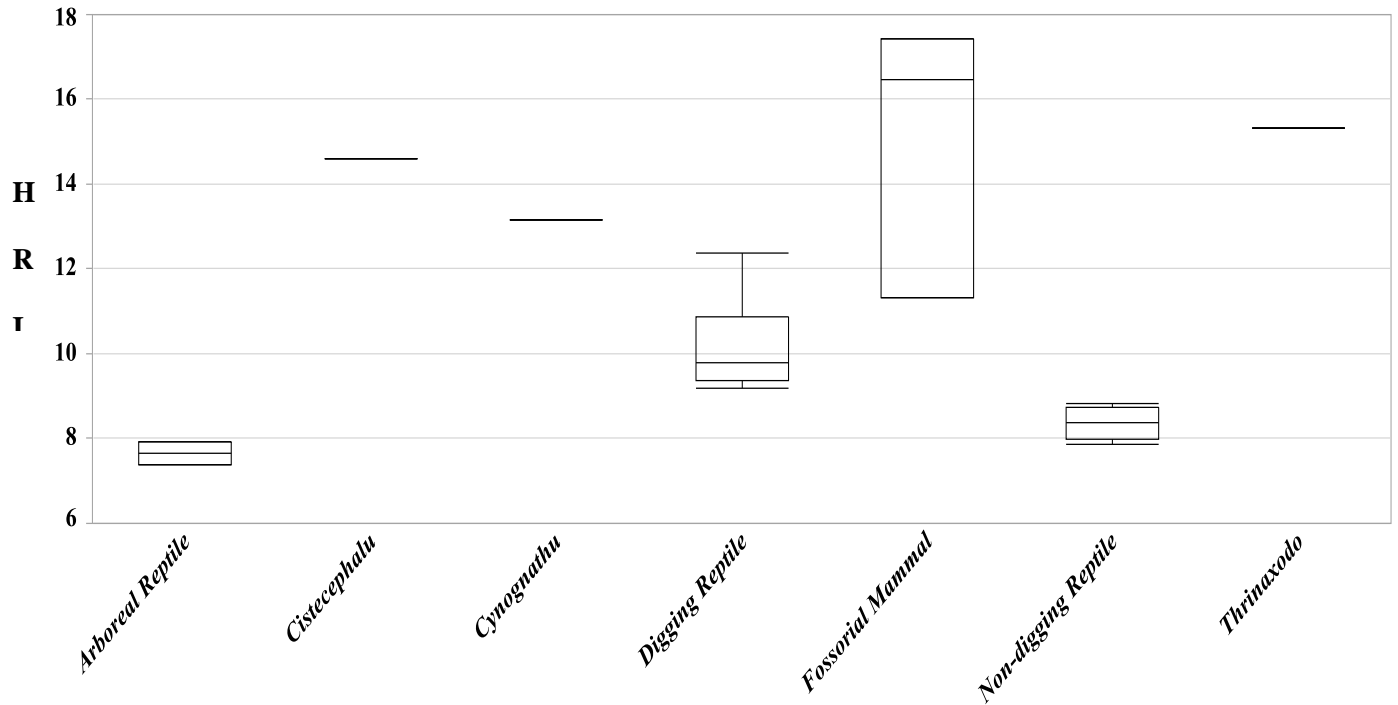


Figure 15: Box plot of the Humerus Robustness Index (HRI) for therapsid fossils, fossorial mammals and reptiles with different locomotor adaptations.

3) Epicondyle Index (EI)

Thrinaxodon has the highest EI of 52.92% followed by *Cynognathus* at 50.31% and *Cistecephalus* at 50.10% (Figure 16, Table A1). The fossorial mammals have an EI ranging between 42.98% and 46.50% (Figure 16). *Anolis equestris*, the arboreal reptiles, have an EI of 23.74% and 24.18% (Figure 16, Table A1). There are only three digging reptiles that have EI % values in the 30s: *Gerrhosaurus validus* at 34.71%, *Varanus niloticus* (specimen VN1) at 37.16% and *Varanus niloticus* (specimen VN2) at 33.64% (Table A1). Amongst the digging reptiles, *Crocodylus moreletti*, has the lowest EI at 20.75% (Table A1). The other reptiles, either digging or non-digging, have EI % values in the 20s (Table A1).

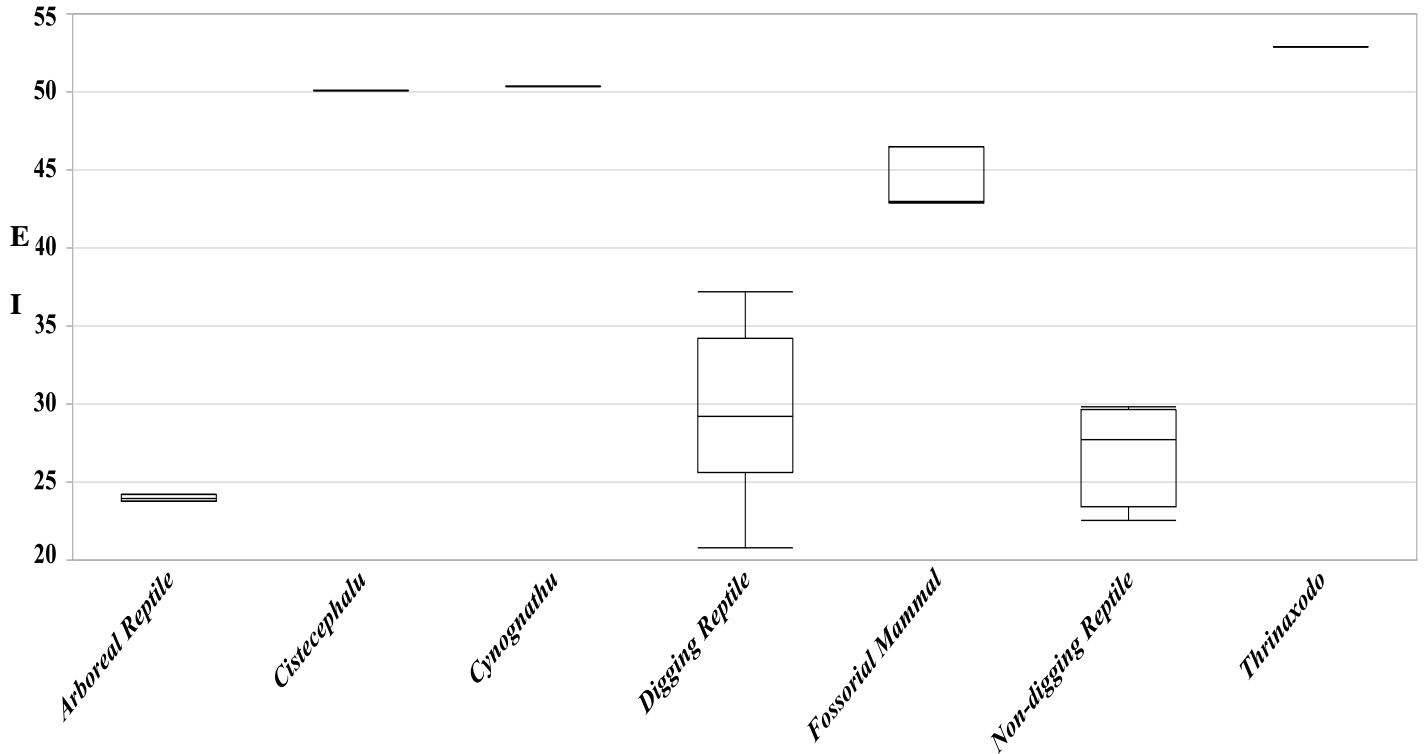


Figure 16: Box plot of the Epicondyle Index (EI) for therapsid fossils, fossorial mammals and reptiles with different locomotor adaptations.

4) Index of Fossorial Ability (IFA)

Thrinaxodon has an IFA of 2.06% and *Cistecephalus* has an IFA of 7.95% (Figure 17).

Lasiorhinus kreffti and *Vombatus* have the highest IFA of 20.40% to 23.11%, respectively (Figure 17, Table A1). Two different individuals of *Cynognathus ulnae* were analysed. The larger ulna had an IFA of 3.60%, while the smaller ulna had an IFA of 2.83% (Figure 17, Table A1). The digging reptiles have an IFA ranging between 1.28% and 4.99%, however, *Crocodylus* (specimen ZA913) has an IFA at 6.50% (Table A1). *Anolis equestris* (specimen R59327) has an IFA of 2.45% and *Anolis equestris* (specimen R59328) has an IFA of 5.63% (Table A1).

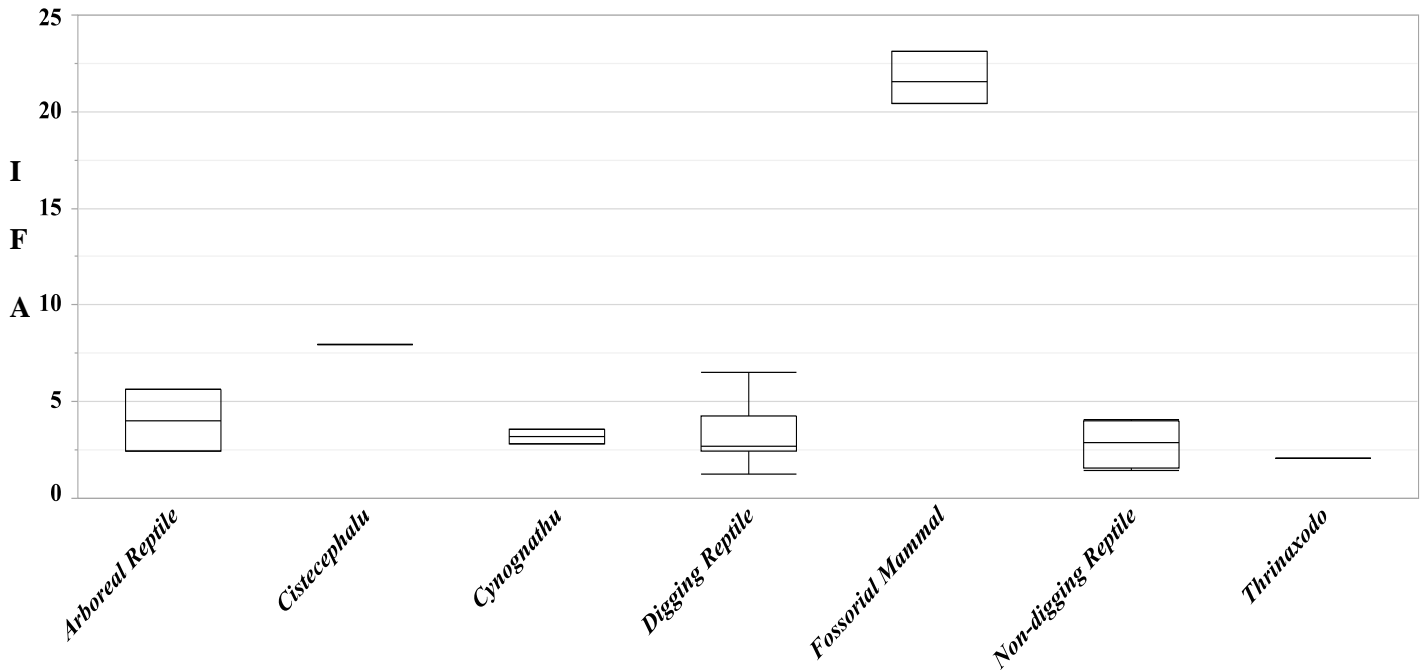


Figure 17: Box plot of the Index of Fossorial Ability (IFA) for therapsid fossils, fossorial mammals and reptiles with different locomotor adaptations.

5) Ulna Robustness Index (URI)

Thrinaxodon has a URI of 6.95% (Figure 18). *Cistecephalus* has the highest URI at 12.64% and *Crocodylus* (specimen ZA913) has the second highest URI at 10.16% (Figure 18, Table A1). *Platysaurus imperator* and *Pseudocordylus melanotus* (specimen R184420) have the lowest URI's of 4.45% and 4.63%, respectively (Table A1). The URI's for fossorial mammals, arboreal reptiles, digging and non-digging reptiles overlap between 5.16% and 9.66% (Figure 18, Table A1).

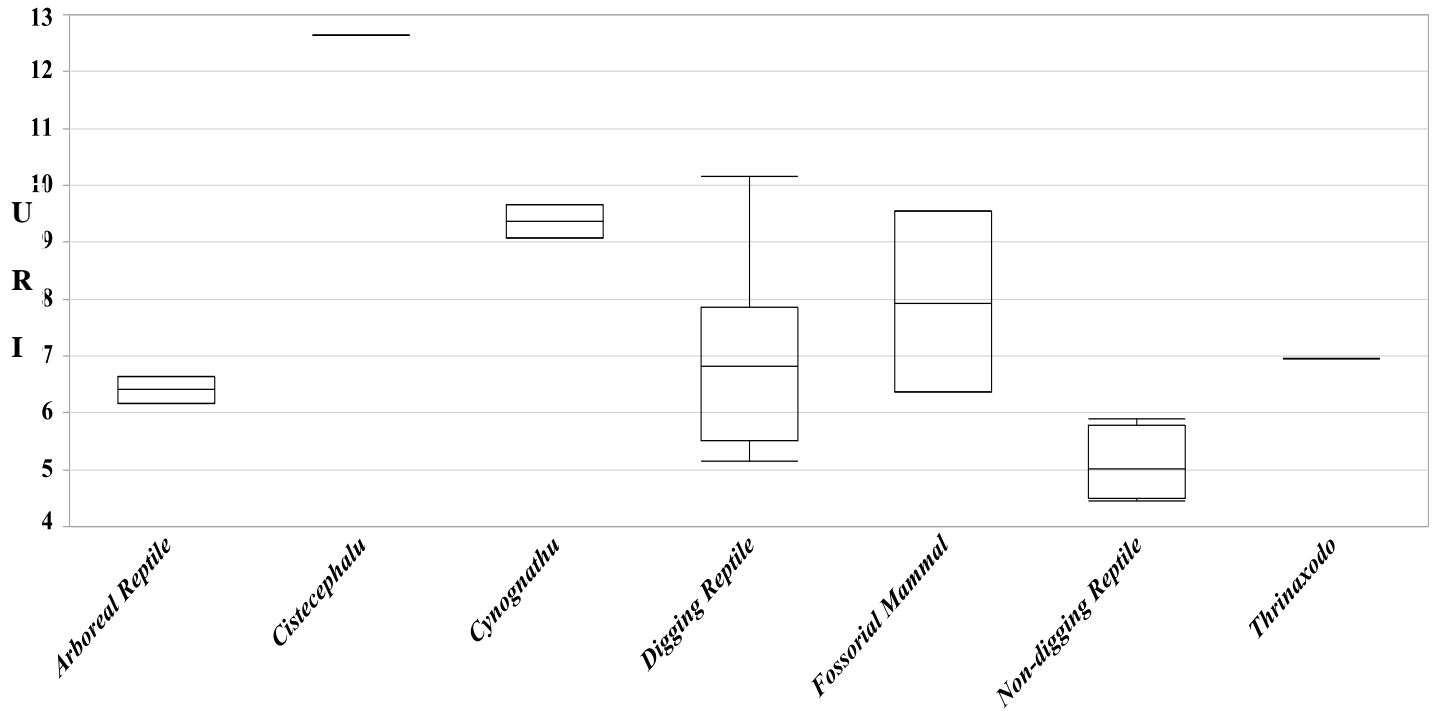


Figure 18: Box plot of the Ulna Robustness Index (URI) for therapsid fossils, fossorial mammals and reptiles with different locomotor adaptations.

Cortical thickness

1) Percentage Cortical Area (%Ct.Ar).

Thrinaxodon exhibits the third highest %Ct.Ar at 89.76% (Figure 19, Table A2). The highest %Ct.Ar is exhibited by the non-digging reptile, *Pseudocordylus melanotus* (specimen R184420), at 94.52% (Table A2). The lowest %Ct.Ar. is exhibited by *Cynognathus* at 49.13% (Figure 19, Table A2). There is overlap amongst the arboreal reptiles, digging reptiles, fossorial mammals and the non-digging reptiles, with a range between 75.02% and 91.12% (Figure 19).

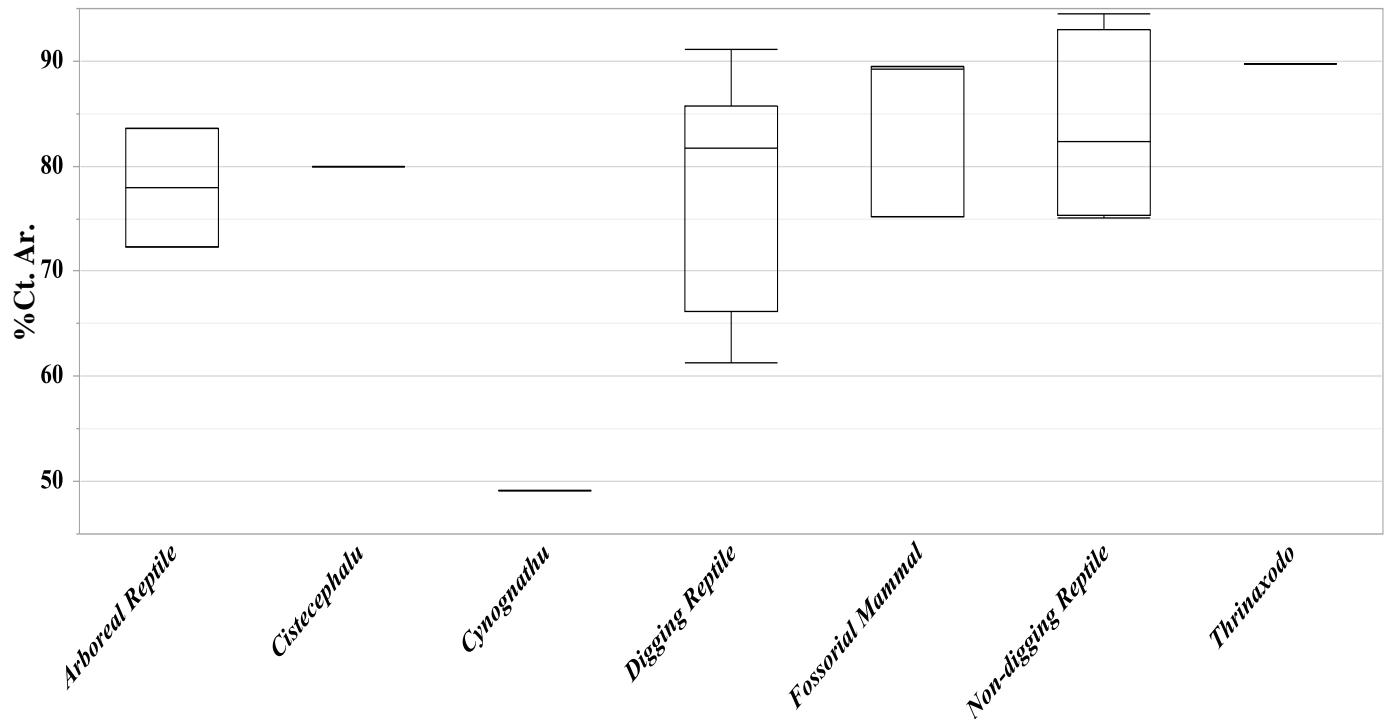


Figure 19: Box plot of the percentage cortical area (%Ct.Ar) for humeral structure at 50% region of interest.

2) Anteroposterior (AP) bending rigidity [I_x (mm^4)]

Thrinaxodon has a scaled I_x at 5.31 mm^4 (Figure 20, Table A2) and the highest (12.70 mm^4) bending in the AP direction was found to be for the digging reptile, *Crocodylus* (specimen ZA913) (Figure 20, Table A2). The arboreal reptiles had the lowest bending in the AP direction at $2.17 - 3.02 \text{ mm}^4$ (Figure 20, Table A2). The non-digging reptiles had a scaled I_x range of $4.19 - 6.19 \text{ mm}^4$ (Figure 20).

3) Mediolateral bending rigidity [I_y (mm^4)]

Thrinaxodon had a ML bending at 5.47 mm^4 (Figure 20). The digging reptiles had the highest bending in the ML (mediolateral) direction at 12.60 mm^4 (Figure 20, Table A2). The arboreal

reptiles had the lowest ML at 2.04 mm⁴. The fossorial mammals had an ML range between 10.50 mm⁴ and 11.27 mm⁴ (Table A2).

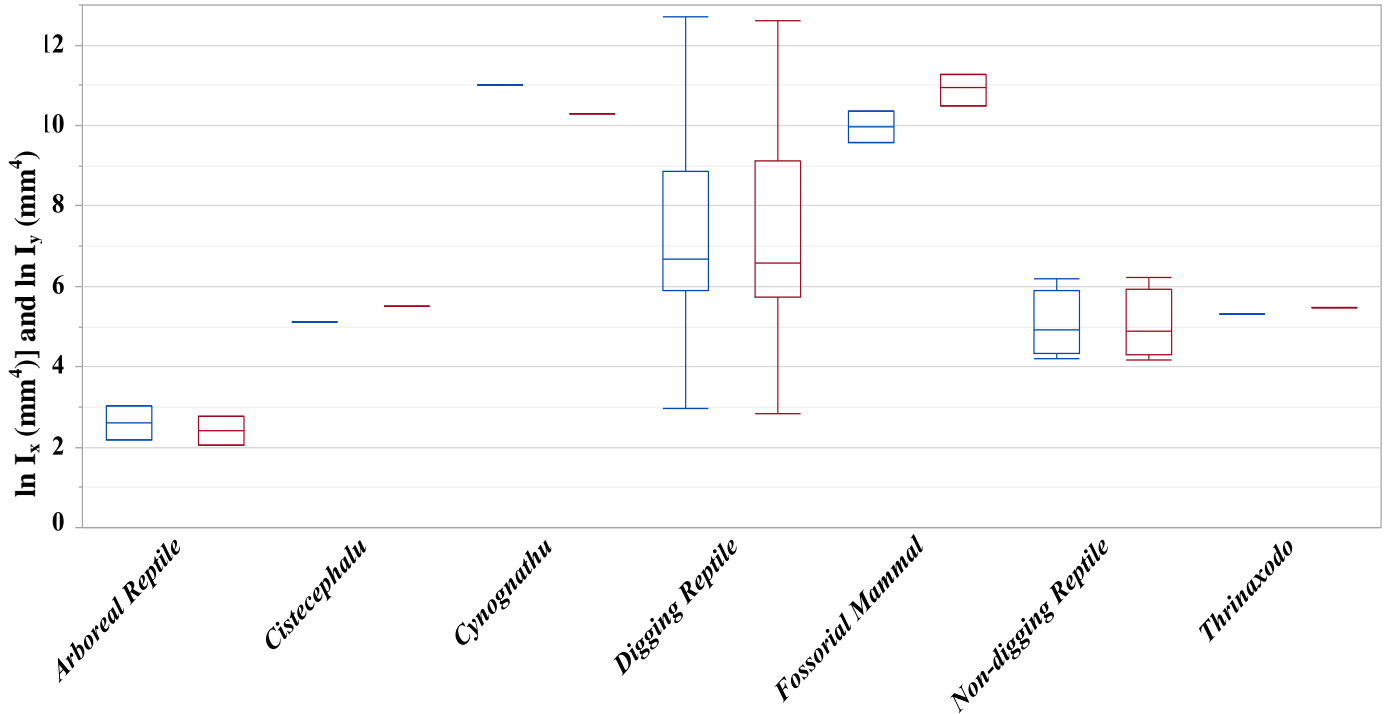


Figure 20: Box plot of the anteroposterior (AP) bending rigidity [$\ln I_x (mm^4)$] and mediolateral bending rigidity [$\ln I_y (mm^4)$] for humeral structure at 50% region of interest. □ - I_x and □ - I_y

Thrinaxodon has an AP that is equal to its ML (Figure 21). The fossorial mammals ML (I_y) are higher than its AP (I_x) (Figure 21). Whereas, *Cynognathus* and *Cistecephalus* have an AP value higher than its ML (Figure 21). Most of the species under investigation have an AP equal to its ML (Figure 21). This illustrates that I_x is a good indicator of I_y , i.e., as I_x increases for a species so does the I_y .

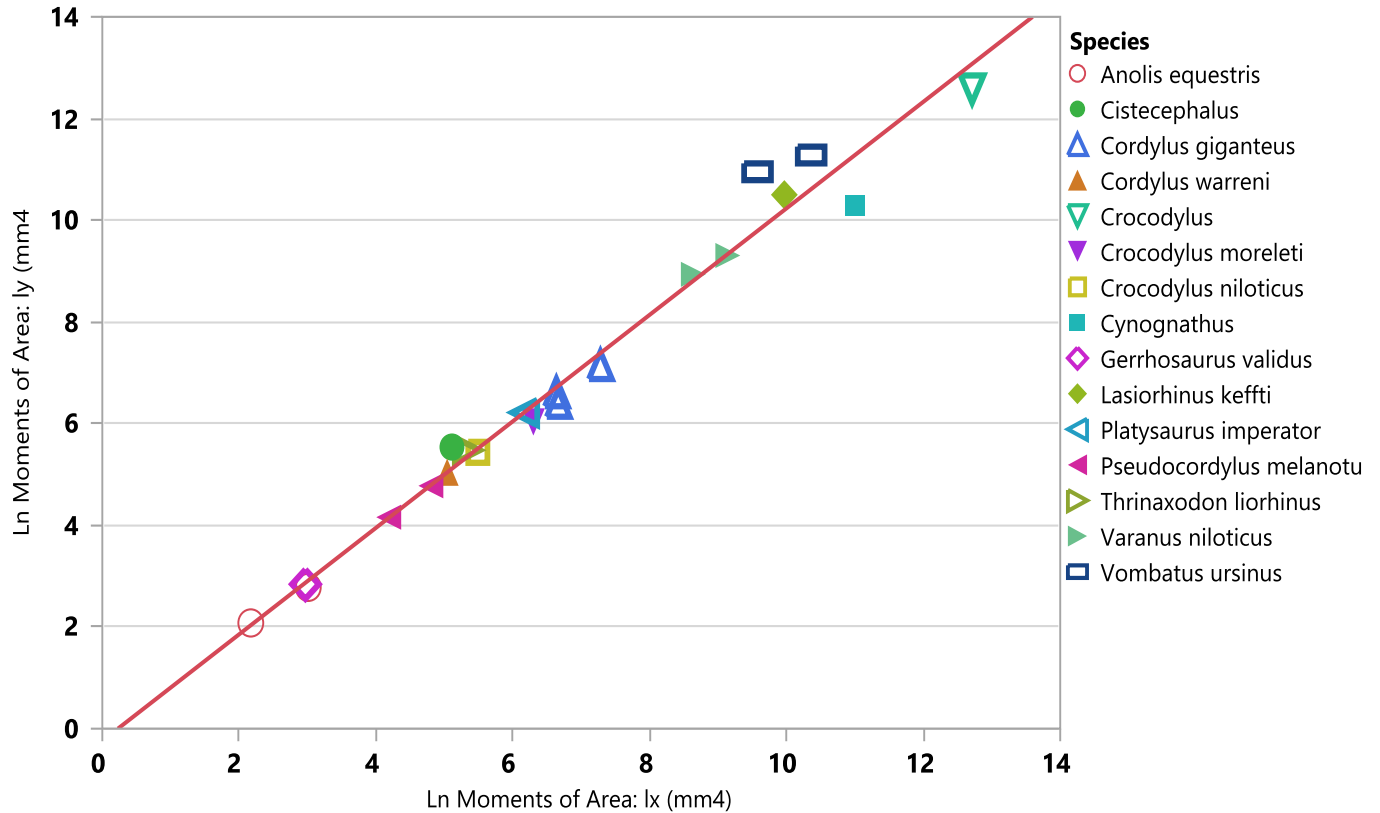


Figure 21: Scatter plot of the anteroposterior (AP) bending rigidity [$\ln I_x (mm^4)$] versus mediolateral bending rigidity [$\ln I_y (mm^4)$] for humeral structure at 50% region of interest, $I_y = -0.239 + 1.047 I_x$, $r^2 = 0.98$, F-ratio = 972.71, $p < 0.0001$

4) Rigidity index (I_y/I_x) and shape ratio (I_{max}/I_{min})

Thrinaxodon had an I_y/I_x of 1.03 and a shape ratio (I_{max}/I_{min}) of 0.93 (Figure 22, Table A2). *Thrinaxodon* overlaps with digging reptiles in the rigidity index and shape ratio (Figure 22). The fossorial mammal, *Vombatus ursinus*A1258, had the highest rigidity index of 1.14 (Figure 22, Table A2). The arboreal reptiles had the lowest rigidity index of 0.92 (Figure 22, Table A2). The highest shape ratio was *Crocodylus* ZA913 of 0.99 and *Anolis equestris* R59327 had the lowest ratio of 0.92 (Figure 22).

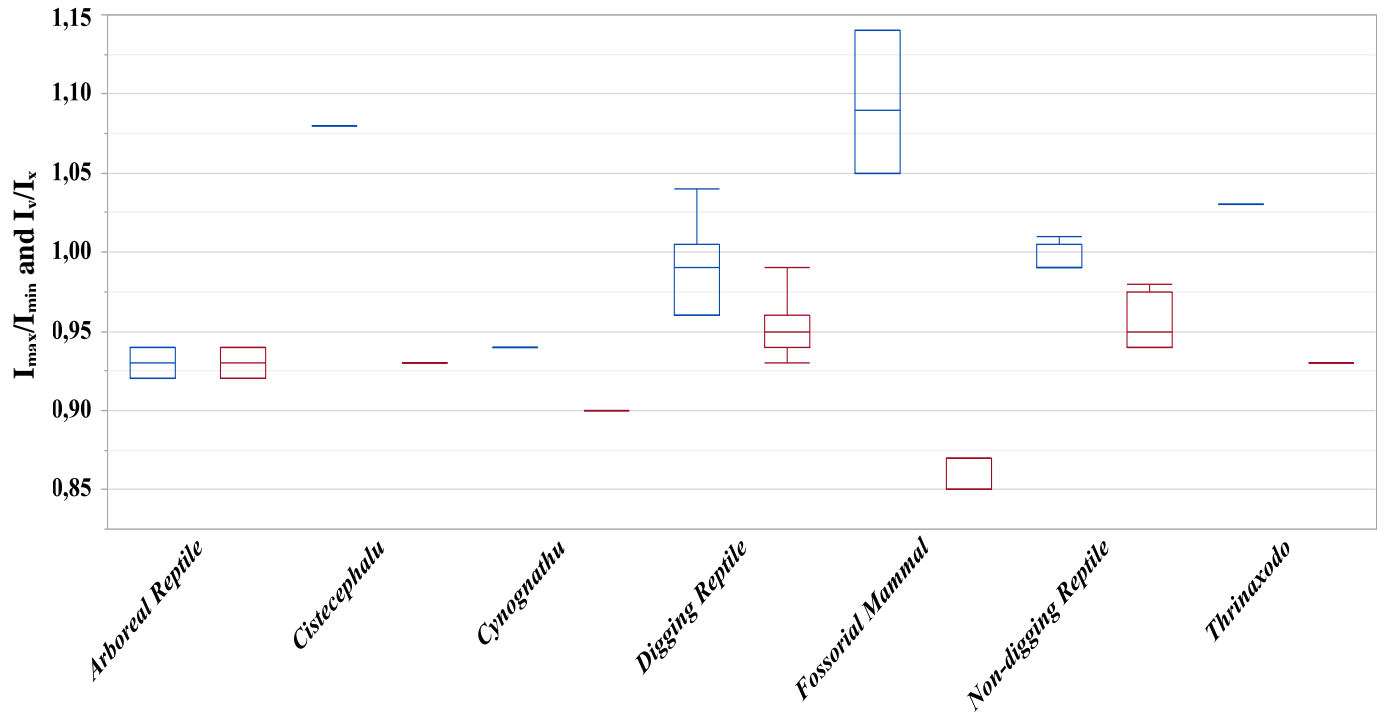


Figure 22: Box plot of the ratio of second moments of area (I_y/I_x and I_{max}/I_{min}) at the midshaft (50%) region of interest. □ - I_{max}/I_{min} and □ - I_y/I_x .

5) Polar moment of area, torsional rigidity (J)

Thrinaxodon had a J at 10.81 mm^4 (Figure 23). The digging reptile, *Crocodylus* (specimen ZA913), had the highest torsion (J) at 25.29 mm^4 and the arboreal reptiles had the lowest J at 4.21 mm^4 (Figure 231, Table A2). *Thrinaxodon* overlaps with the digging reptiles (Figure 23).

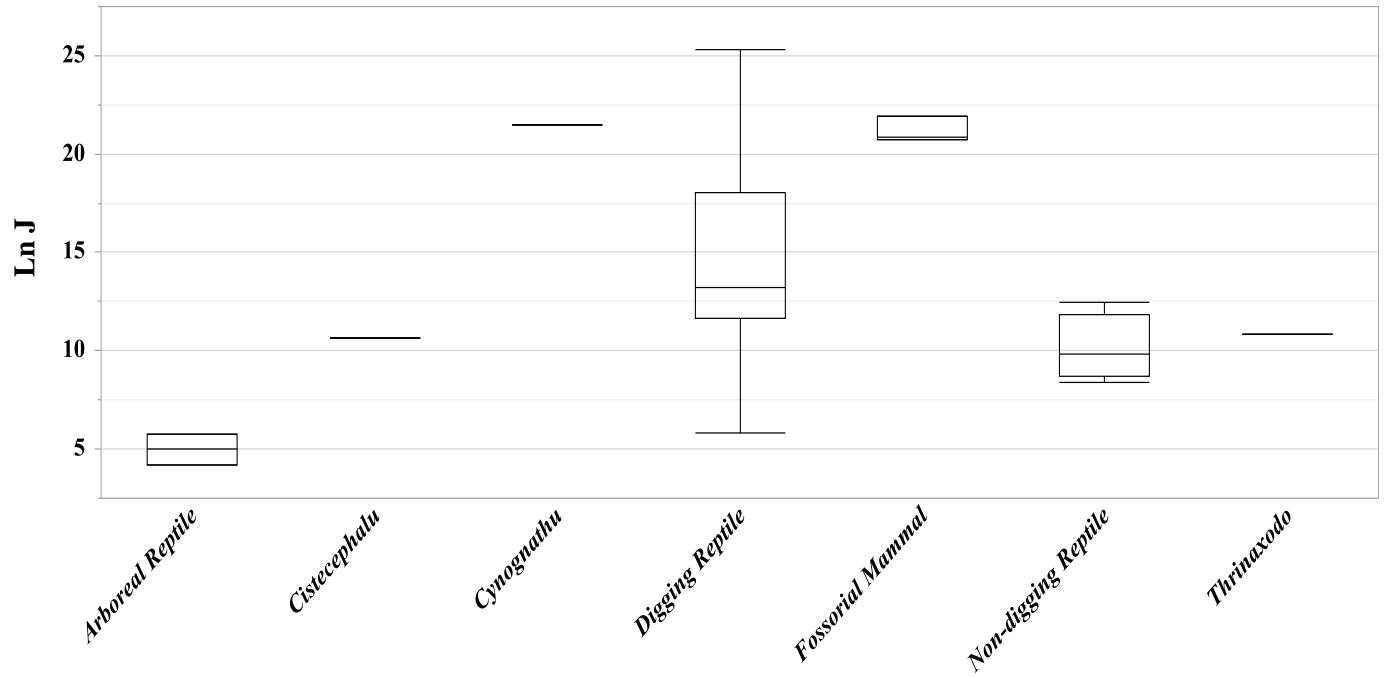


Figure 23: Box plot of the polar moment of area, torsional rigidity ($\ln J$) for humeral structure at 50% region of interest.

6) Average bending rigidity ($J/2$)

Thrinaxodon had a $J/2$ at 5.41 (Table 2A). The highest value ($J/2$) was exhibited by the digging reptile, *Crocodylus* (specimen ZA913) (Figure 24) at 12.65 (Table 2A). And the lowest bending rigidity was found to be for the arboreal reptiles at 2.11 (Figure 24).

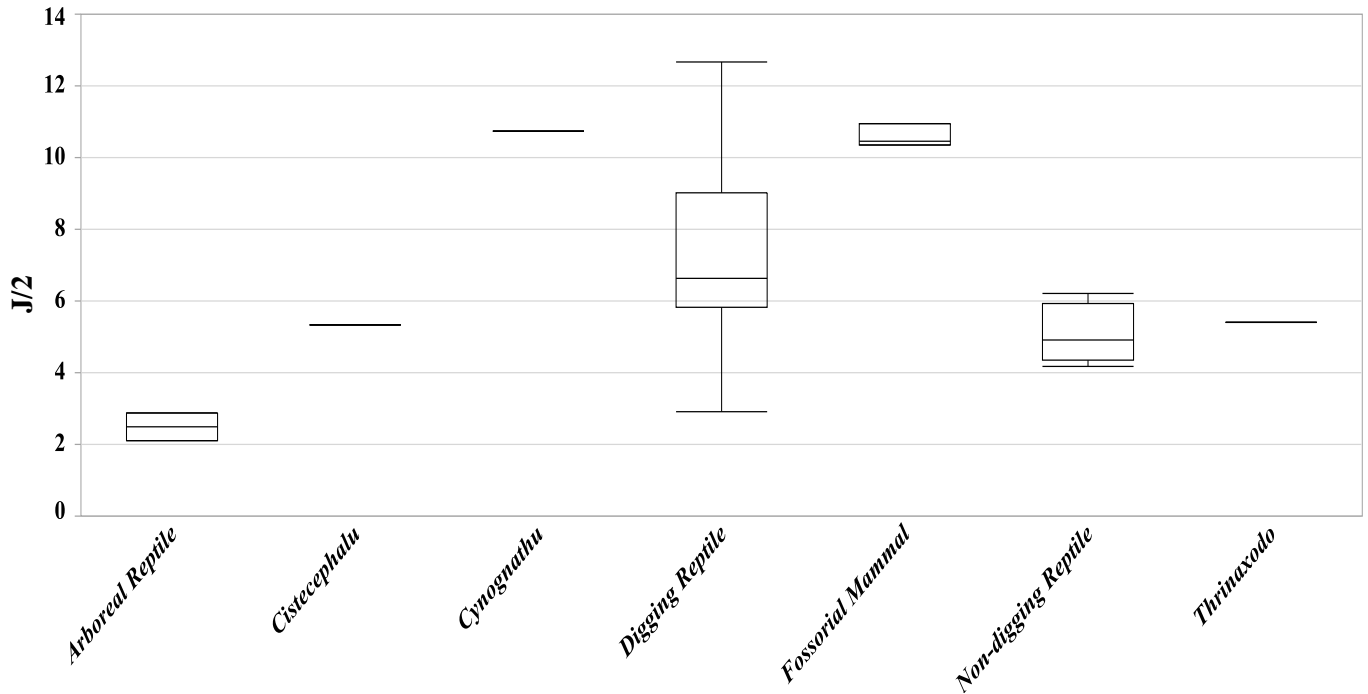


Figure 24: Box plot of the average bending rigidity ($J/2$) for humeral structure at 50% region of interest.

Torsion

Thrinaxodon has the highest torsion with an angle of 73.88° (Figure 25). Fossorial mammals have an average torsion angle between 38.90° and 39.31° (Figure 25). *Cistecephalus* has a torsion angle of 44.45° which is the lowest angle amongst the fossil species under investigation (Figure 25). Reptilian diggers have an angle ranging from 7.38° to 44.50° (Figure 25). From the four non-digging reptiles, three species have angles ranging between 38.11° and 46.93° , while the fourth species (i.e., *Platysaurus imperator*) has an angle of 72.22° (Figure 25). The two arboreal specimens, *Anolis equestris*, have an angle of 48.89° and 70.80° (Figure 25).

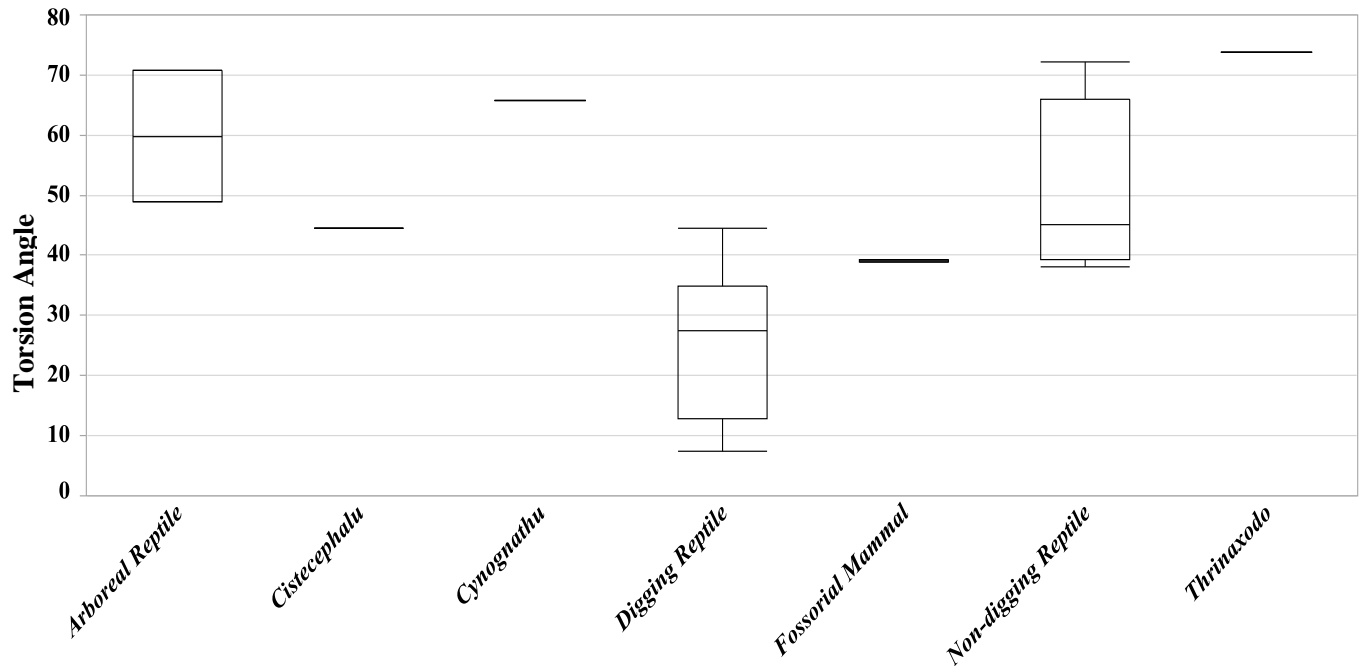


Figure 25: Box plot of the torsion angle for fossil species and extant species where the latter are grouped into behavioural categories.

Discussion

General configuration

The general shape of the *Thrinaxodon* humerus resembles that of fossorial species whether being fossorial mammals or digging reptiles. This morphology relies on the fact that the epiphyseal ends are both broad with slight torsion of the shaft which is a typical morphological characteristic of diggers (Jenkins 1973; Kemp 1980; Kardong 2002; Sanchez-Villagra *et al.* 2004; Meier *et al.* 2013). *Thrinaxodon* humerus shape is closest to that of fossorial mammals and furthest away from the arboreal reptiles along PC1 (Figure 2). The humeral displacement (Figure 3) illustrates that the deltopectoral crest decreases from fossorial to arboreal species. The decline in width of the deltopectoral crest reduces the area that is available for muscle attachment. Musculoskeletal anatomy of the fossorial mammals as well as the

digging reptiles is specialised for joint stability and increased force during activity (Grand and Barboza 2001). Fossorial species require powerful muscles that are attached to broad bony structures (Turnbull and Reed 1967) on the epiphyses and short robust diaphyses (Warburton *et al.* 2013). These muscles are needed in relation to the type of digging behaviour the species exhibits. The shortness of forelimb bones relative to the body increases the mechanical advantage of attaching muscles during a function such as digging (Hildebrand and Goslow 2001).

The SMI provides an indication of how efficient the deltoid muscle is in relation to the bone (Elissamburu and De Santis 2011). This index measures the area that is available for attachment of the *M. deltoideus*. The longer the length of the deltopectoral crest in relation to the humeral length, the more efficient the mechanical advantage of the deltoid will be (Elissamburu and De Santis 2011). *Lasiorhinus kreffti* is a well-known fossorial mammal that has the highest mechanical advantage when compared to the other extant species under investigation (Figure 14, Table A1). The SMI provides evidence of humeral stability for body support and digging activity. The SMI for *Cynognathus* was over 50% and was similar to that of *Thrinaxodon* and the fossorial mammal (Figure 14). This may reflect their large body size and accounts for the stability of the body rather than the fossorial behaviour. *Cistecephalus* SMI is very similar to that of digging reptiles and supports the assumption of fossorial behaviour for the dicynodont (Figure 14). *Thrinaxodon* exhibited an average SMI that demonstrates the mechanical advantage of its deltoid to be close to that of fossorial mammals (Figure 14).

Overlap along PC1 in quadrant 1 (positive x-axis and positive y-axis), verify that the digging and non-digging reptiles, to some extent, share similarities in their humeral shape (Figure 2). Even though *Cordylus giganteus* is a digging reptile and *Cordylus warreni* is a non-digging reptile, there is evidence that they share shape (PC1) and width size (PC2) similarities in their humeri (Figure 2). This is in relation to the specimens being in the same genus but different species. The width of the flexor, pronator and supinator of the antebrachium is indicated by the EI (Elissamburu and De Santis 2011). *Thrinaxodon* had the highest EI with close values for the humerus of *Cynognathus* and *Cistecephalus* (Figure 16), which

indicates the area available for larger muscle attachment. The expansion of the distal humerus seen in the fossils (Figure 16) may be related to the semi-sprawling posture evident in therapsids. The epiphyseal ends are affected by the functional activity of the forelimb (Szalay 1994) and thus, most muscle attachments, whether the origin or insertion, occur at the extreme ends. The other reptiles species, digging and non-digging, ranged between 20% and 30% (Figure 16, Table A1). This illustrates that the width of the epicondyle in relation to the length of the humerus is relative to the digging function as well as to body support (Elissamburu and Vizcaino 2004).

For the radius, *Thrinaxodon* does not overlap with any of the species along PC1 and PC2, however, it does lie in the same quadrant as *Cistecephalus*, *Cynognathus* and *Crocodylus* (Figure 6). This reveals separation of the therapsid fossils with the extant species, i.e., evidence of a phylogenetic relationship. The radius bears a fraction of the body weight (Argot 2001) and thus explains that *Thrinaxodon* having semi-sprawled limbs share minimal similarities to reptiles that are sprawled limbed. The difference between the radii is given by the width of the radial shaft (Figure 7, Figure 9). However, it should be noted that radii are structurally columnar and may not reveal many structural differences amongst species. The enlarged area for muscle attachment is necessary to be able to withstand resistance from the ground during digging (Warburton *et al.* 2013). The arboreal species overlap with the non-digging reptiles along PC1 and with the digging reptiles along PC2 (Figure 6). This is likely related to the fact that all reptiles share similarities in limb structure. The fossorial mammals overlap with digging and non-digging reptiles along PC3, which accounts for something other than shape and size (Figure 8).

The *Thrinaxodon* ulna lies closest to that of extant reptiles along PC1 (Figure 10), and illustrates that fossorial mammals are an outlier in ulnar structure. This is due to mammals possessing a prominent olecranon process that is absent in reptiles. The structure of the ulna, for the fossils and the reptiles except *Varanus*, has a posterior proximal facet behind the articular facet and this structure would have the function of the olecranon process. *Varanus* species have a small protruding structure on the posterior portion of the proximal end. From the analyses of the extant *Varanus* ulna, this structure is not completely

ossified on the proximal epiphyseal end and suggests that either it may not have been fossilised in *Thrinaxodon*, *Cynognathus* or *Cistecephalus* (e.g., not ossified), or it may have been absent. This small bony process may account for the slight overlap along PC2 between the fossorial mammals and digging reptile, *Varanus* (Figure 10) and could possibly explain a phylogenetic relationship. The fossil species, however, may have had a cartilaginous olecranon or it could have been completely absent (Iqbal 2013). Having said this, the extant reptilian species retained their primitive structure in the ulna and overlap along PC1 (Figure 10).

The IFA is in relation to the mechanical advantage of the triceps that are attached to the olecranon process of the ulna (Elissamburu and De Santis 2011). This index is a good statistic of fossoriality as it reflects force development for digging (Hildebrand 1985; Vizcaino *et al.* 1999; Vizcaino and Milne 2002; Elissamburu and De Santis 2011). However, due to the reptilian species lacking an olecranon, there is overlap between the reptilian diggers and non-diggers (Table A1). The fossorial mammals have the highest IFA and *Thrinaxodon* has the lowest (Figure 17). Due to the lack of an olecranon and the difference in width of the epiphyseal ends, IFA may not provide enough information to the extent of *Thrinaxodon* exhibiting fossorial or reptilian features.

The PC1 ulna displacement (Figure 11) illustrates the decline of the olecranon process on the proximal end, whereas the PC2 (Figure 13) explains the decrease in anteroposterior length along the ulna shaft. The indication of the ulna robustness is given by URI and is in relation to the insertion of muscles involved in pronation and supination of the antebrachium (Elissamburu and De Santis 2011). The highest URI are the fossorial mammals, digging reptiles, *Cistecephalus*, *Cynognathus* and *Thrinaxodon* (Figure 18). This evidence proves that there is an increase in robusticity among the species from non-digging reptiles to fossorial mammals (Figure 18). The URI can be used to distinguish among the different types of digging activity in species (Elissamburu and De Santis 2011).

Internal morphology

Cortical bone thickness responds to the activity the bone endures (Meier *et al.* 2013). It was stated by Magwene (1993), that non-mammalian therapsids had less dense bones as they were subjected to greater bending and torsion levels (Botha 2003). However, *Cistecephalus* and *Thrinaxodon* exhibited %Ct.Ar that overlapped with extant species (Figure 19, Table A2). HRI provides a signal for the robustness of the humerus. This index is related to digging activity and body support during a function (Elissamburu and Vizcaino 2004; Elissamburu and De Santis 2011). When compared to all species, *Thrinaxodon* paired closely to the fossorial mammals with 15.33% robustness (Figure 15) and 3% more than the digging reptiles (Table A1).

Depending on the type of burrower, the humeral diaphysis is either rounded or flattened anteroposterior (I_x) (Turnbull and Reed 1967). The increase in AP and ML, relates to the more strain that is applied to the bone (Carlson 2014). The fossorial mammals have the highest AP and ML, followed by *Cistecephalus*, *Cynognathus* and the digging reptiles (Figure 20, Figure 21). This would suggest that the digging species have a higher activity lifestyle than non-diggers or arboreal species. As the bone shortens proximodistally, it widens mediolaterally at its epiphyses, which allows for the enlarged muscle attachment areas of wrist flexors and extensors. *Thrinaxodon* (Figure 25) and the fossorial mammals (Figure 23) both exhibit high torsion angles. However, the fossorial torsion angles overlap with the non-digging and arboreal species. This may explain that torsion observed in extant reptiles is directly related to their sprawling posture. It has been stated in previous research that cortical thickness and torsion have a corresponding relationship (Evans 1978). The cortical thickness and torsion statistical evidence alone supports the hypothesis that *Thrinaxodon* exhibit fossorial-like morphology in the forelimb.

Limitations

The mass of each muscle was not reported for and through literature it is apparent that this weight as well as size in relation to the other muscles plays a role in whether the muscle attached to the bone is

well adapted for the function. As the muscle size differs across locomotor ability, the extent to which the muscle functions in the specific activity is unknown, i.e., the muscle mass would increase from arboreal to fossorial species. To account for this, a dissection from each behavioural category should be undertaken, where the muscles mass in relation to the bone should be noted.

Some of the fossil taxa's humeral medullary space may have been filled with sediment which revealed little to no space in the centre during digital segmentation. And this demonstrated difficulties as the cavity was needed for the analyses of the cross sectional properties. To overcome the difficulty in visualising the medullar cavity, it may be advised to have a histological analyses for the cortical structure.

There have been many observational studies on the different types of digging behaviour in extant species and these assumptions have been made for the fossil taxon. However, the type of digging behaviour exhibited in the fossil form will remain unknown. The extent of digging may be better understood by incorporating the manus and hindlimb into research.

Conclusions

The research conducted aimed to examine the extent to which the *Thrinaxodon* forelimb reflects fossorial morphology or forms of reptilian gait. Ultimately, the morphology supported that *Thrinaxodon* forelimb morphology is close to that of fossorial mammals. However, due to the semi-sprawled limb posture, *Thrinaxodon* does share minimal forelimb modifications with reptiles in order to keep its trunk (body) from dragging on the ground. The musculoskeletal anatomy of *Thrinaxodon* displays adaptations to a fossorial lifestyle and as being the transitional species from a reptilian phase to a parasagittal gait as seen in extant fossorial mammals. The goal of this study was to enhance insight into the functional morphology of *Thrinaxodon* forelimb through comparisons with species of different locomotor behaviour, which was investigated by analyses of the indices, the PCA, and the internal and external examination. There are true differentiations between the reptilian and mammalian forelimb. However, there is evidence of gradual change among the synapsid group (*Cistecephalus*, *Thrinaxodon* and

Cynognathus) to illustrate these changes from the primitive state to a modern state, i.e., from reptilian to mammalian. Cynodonts exhibit a primitive sprawling or semi-sprawling gait and the musculoskeletal similarities to reptiles are postural rather than behavioural. Analyses of more therapsid species, which includes the hindlimb, would permit a more comprehensive interpretation of the locomotion, gait and behaviour among the species. This study provided direct anatomical evidence that the limb configuration of *Thrinaxodon* indicates the non-mammalian forelimb form had begun to show similarities to the mammalian form.

Acknowledgements

I sincerely thank my advisors, Dr. Kristian Carlson and Dr. Fernando Abdala, for providing support, assistance, guidance and expertise. This research was funded by The Palaeontological Scientific Trust (PAST) and its Scatterlings of Africa programmes as well as the National Research Foundation (NRF). I gratefully wish to thank Dr. Tea Jashashvili for all her assistance and expertise on helping and guiding me on the torsion method, Avizo, VG Studio Max, Morphologika, MorpholTools and JMP. I humbly wish to thank Prof. Paul Manger and Mr. Brendon Billings (School of Anatomical Sciences, University of the Witwatersrand) for their help in organising the dissection material for this research. A thank you goes to Dr. Jonah Chioneire and Miss Casey Staunton for help on Inkscape 0.48 and Prof. Graham Alexander for guidance on the reptilian species. The curators and collection managers of the following institutions are acknowledged for allowing access to their specimens: ESI, APES, SAS, DNMNH, MCZ, ANWC, QM and TM. I would also like to thank the University of the Witwatersrand and the Evolutionary Studies Institute for the opportunity to conduct this research.

References:

- ABDALA, F. and RIBEIRO, A. M. 2010. Distribution and diversity patterns of Triassic cynodonts (Therapsida, Cynodontia) in Gondwana. *Palaeogeography, Palaeoclimatology, Palaeoecology* **286**: 202-217.
- ABDALA, V. and MORO, S. 2006. Comparative mycology of the forelimb of *Liolaemus* sand lizards (Liolaemidae). *Acta Zoologica (Stockholm)* **87**: 01-12.
- ABDALA, V. and DIOGO, R. 2010. Comparative anatomy, homologies and evolution of the pectoral and forelimb musculature of tetrapods with special attention to extant limbed amphibians and reptiles. *Journal of Anatomy* **217**: 536-573.
- ALEXANDER, G. and MARAIS, J. 2007. *A guide to the reptiles of Southern Africa*. Struik Publishers. Cape Town. South Africa.
- ARGOT, C. 2001. Functional-adaptive anatomy of the forelimb in the didelphidae, and the paleobiology of the Paleocene marsupials *Mayulestes ferox* and *Pucadelphys andinus*. *Journal of Morphology* **247**: 51-79.
- BLOB, R. W. 2001. Evolution of Hindlimb posture in Nonmammalian Therapsids: Biomechanical Tests of Palaeontological Hypotheses. *Palaeontology* **27**: 14-38.
- BLOB, R. W. and BIEWENER, A. A. 1999. *In vivo* locomotor strain in the hindlimb bones of *Alligator mississippiensis* and *Iguana iguana*: implications for the evolution of limb bone safety factor and non-sprawling limb posture. *The Journal of Experimental Biology* **202**: 1023-1046.
- BORDY, E. M., SZTANO, O., RUBIDGE, B. S. and BUMBY, A. 2009. Tetrapod burrows in the southwestern main Karoo Basin (Lower Katberg Formation, Beaufort Group), South Africa. *Palaeontologica Africana* **44**: 95-99.

- BOTHA, J. 2003. Biological aspects of the Permian dicynodont *Oudenodon* (Therapsida: Dicynodontia) deduced from bone histology and cross-sectional geometry. *Palaeontologica Africana* **39**: 37-44.
- BOTHA, J., LEE-THORP, J. and SPONHEIMER, M. 2004. An examination of Triassic Cynodont tooth enamel chemistry using Fourier Transform Infrared Spectroscopy. *Calcified Tissue International* **74**: 162-169.
- BOTHA, J., ABDALA, F. and SMITH, R. 2007. The oldest cynodont: new clues on the origin and early diversification of the Cynodontia. *Zoological Journal of the Linnean Society* **149**: 477-492.
- BRANCH, B. 1998. *Field guide to Snakes and other reptiles of Southern Africa*. Struik Publishers. Cape Town. South Africa.
- CARLSON, K. J., JASHASVILI, T., HOUGHTON, K. WESTAWAY, M. C. and PATEL, B. A. 2013. Joint loads in marsupial ankles reflect habitual bipedalism versus quadrupedalism. *PLOS One*. **08**: 01-09.
- CARLSON, K. J. 2005. Investigating the form-functional interface in African apes, relationships between principal moments of area and positional behaviours in femoral and humeral diaphyses. *American Journal of Physical Anthropology* **127**: 312-334.
- CARLSON, K. J. 2014. Linearity in the Real World: An experimental assessment of nonlinearity in terrestrial locomotion. Chapter 14. In: CARLSON, K. J. and MARCHI, D. (eds) *Reconstructing Mobility: Environmental, Behavioural, and Morphological Determinants*. Springer. New York. United States of America.
- CLUVER, M. A. 1978. The skeleton of the mammal-like reptile *Cistecephalus* with evidence for a fossorial mode of life. *Annals of The South African Museum* **76**: 213-246.

- DAMIANI, R., MODESTO, S., YATES, A. and NEVELING, J. 2003. Earliest evidence of cynodont burrowing. *Proceedings of the Royal Society of London: Biological Sciences* **270**: 1747-1751.
- ELISSAMBURU, A. and VIZCAINO, S. F. 2004. Limb proportions and adaptations in caviomorph rodents (Rodentia: Caviomorpha). *Proceedings of the Zoological Society of London, Journal of Zoology* **262**: 145-159.
- ELISSAMBURU, A. and DE SANTIS, L. 2011. Forelimb proportions and fossorial adaptations in the scratch-digging rodent *Ctenomys* (Caviomorpha). *Journal of Mammalogy* **92**: 683-689.
- EVANS, F. G. 1978. Relations between torsion properties and histology of adult human compact bone. *Journal of Biomechanics* **11**: 157-165.
- FERNANDEZ, V., ABDALA, F., CARLSON, K. J, COOK, D. C., RUBIDGE, B. S., YATES, A. and TAFFOREAU, P. 2013. Synchrotron Reveals Early Triassic Odd Couple: Injured Amphibian and Aestivating Therapsid Share Burrow. *PLOS One* **08**: 01-07.
- GRAND, T. I. and BARBOZA, P. S. 2001. Anatomy and development of the koala, *Phascolarctos cinereus*: an evolutionary perspective on the superfamily Vombatoidea. *Anatomy of Embryology* **203**: 211-223.
- HILDEBRAND, M. 1985. Digging in quadrupeds. *Functional vertebrate morphology*. Belknap Press. Cambridge. United Kingdom.
- HILDEBRAND, M. and GOSLOW, G. E. J. 2001. *Analysis of Vertebrate Structure*. John Wiley and Sons, Inc. New York. United States of America.
- HOPSON, J. A. 1987. The mammal-like reptiles: A study of transitional fossils. *The American Biology Teacher* **49**: 16-26.

- IQBAL, S. 2013. Comparative study of the forelimb of the Early Triassic cynodont *Thrinaxodon liorhinus*: Exploring burrowing anatomy. BSc Honours Thesis. University of the Witwatersrand, Johannesburg, South Africa.
- IQBAL, S., CARLSON, K. J., ABDALA, F. and FERNANDEZ, V. in prep. Fossorial adaptations in the forelimb of the Early Triassic cynodont *Thrinaxodon liorhinus*. Intended for *Journal of Morphology*.
- JASHASHVILI, T., LEBRUN, R. and CARLSON, K. J. 2011. *Variation in morphology and torsion patterns of metatarsals in Pan*. The 80th annual meeting of the American Association of Physical Anthropologists, Minnesota. Minneapolis. United States of America. April 12-16, pg. 177.
- JENKINS, F. A. 1971. The postcranial skeleton of African cynodonts: Problems in the early evolution of the mammalian postcranial skeleton. *Bulletin of the Peabody Museum of Natural History* **36**: 1-216.
- JENKINS, F. A. Jr. 1973. The functional anatomy and evolution of the mammalian humero-ulnar articulation. *American Journal of Anatomy* **137**: 281–298.
- KARDONG, K. V. 2002. *Vertebrates: Comparative Anatomy, function, evolution*. McGraw-Hill. New York. USA.
- KARDONG, K. V. 2009. *Vertebrates: Comparative Anatomy, function, evolution*. Sixth Edition. McGraw-Hill. New York. USA.
- KEMP, T. S. 1980. The primitive cynodont *Procynosuchus*: structure, function and evolution of the postcranial skeleton. *Philosophical Transactions of the Royal Society of London Biological Sciences* **288**: 217-258.

- KEMP, T. S. 1983. The relationships of mammals. *Zoological Journal of the Linnean Society* **77**: 353-384.
- KEMP, T. S. 2005. *The origin and evolution of mammals*. Oxford University Press. Oxford. New York. United States of America. Pp. 60-74.
- LAMPING, B. 2012. *The inquisitive thief*. University of Wisconsin. Milwaukee. United States of America.
- LEBRUN, R. 2008. *Evolution and development of the strepsirrhine primate skull*. Double Doctorate. University of Zurich. Switzerland.
- LEBRUN, R., De LEON, M. P., TAFFOREAU, P. and ZOLLIKOFER, C. 2010. Deep evolutionary roots of strepsirrhine primate labyrinthine morphology. *Journal of Anatomy* **216**: 368-380.
- LIEBERMAN, D. E., POLK, J. D. and DEMES, B. 2004. Predicting long bone loading from cross sectional geometry. *American Journal of Physical Anthropology* **123**: 156-171.
- LUO, Z. and CROMPTON, A. W. 1994. Transformation of the quadrate (Incus) through the transition from non-mammalian Cynodonts to mammals. *Journal of Vertebrate Palaeontology* **14**: 341-374.
- MAGWENE, P. M. 1993. *What's bred in the bone: histology and cross-sectional geometry of mammal-like reptile long bones-evidence of changing physiological and biomechanical demands*. Unpublished MSc thesis. Harvard University. Cambridge. United States of America.
- MEERS, M. B. 2003. Crocodylian forelimb musculature and its relevance to Archosauria. *The Anatomical Record Part A* **274A**: 891-916.
- MEIER, P. S., BICKELMANN, C., SCHEYER, T. M., KOYABU, D. and SANCHEZ-VILLAGRA, M. R. 2013. Evolution of bone compactness in extant and extinct moles (Talpidae): exploring humeral microstructure in small fossorial mammals. *BMC Evolutionary Biology* **13**: 01-10.

- MILNE, N., VIZCAINO, S. F. and FERNICOLA, J. C. 2009. A 3D geometric morphometric analysis of digging ability in the extant and fossil cingulated humerus. *Journal of Zoology* **278**: 1-09.
- MASTERLACK, T., CANOVILLE, A. and CHINSAMY, A. 2013. New insights into the biology of the Permian genus *Cistecephalus* (Therapsida, Dicynodontia). *Journal of Vertebrate Palaeontology* **32**: 1396-1410.
- NICHOLSON, K. E. and RICHARDS, P. M. 2011. Home range size and overlap within an introduced population of the Cuban Knight Anole, *Anolis equestris* (Squamata: Iguanidae). *Phyllomedusa* **1**: 65-73.
- PALMER, D. 1999. *The Marshall illustrated Encyclopedia of dinosaurs and prehistoric animals*. Marshall Editions. London. England.
- O' NEILL, M. C. and RUFF. 2004. Estimating human long bone cross-sectional geometric properties: a comparison of noninvasive methods. *Journal of Human Evolution* **47**: 221-235.
- REILLY, S. M. and DELANCEY, M. J. 1997. Sprawling locomotion in the lizard *Sceloporus clarkia*: quantitative kinetics of a walking trot. *The Journal of Experimental Biology* **200**: 753-765.
- RUBIDGE, B. S. 1995. Biostratigraphy of the Beaufort Group (Karoo Supergroup): *South African Committee for Stratigraphy Biostratigraphy Series*. Department of Mineral and Energy Affairs, Geological Survey **1**: 45.
- RUBIDGE, B. S. 2005. Re-uniting lost continents: Fossil reptiles from the ancient Karoo and their wanderlust. *South African Journal of Geology* **108**: 135-172.
- RUBIDGE, B. S. and SIDOR, C. A. 2001. Evolutionary patterns among Permo-Triassic Therapsids. *Annual Review of Ecology and Systematics* **32**: 449-480.

- RUFF, C. B. and LARSON, C. S. 2014. Long bone structural analyses and the reconstruction of Past mobility: a historical review. Chapter 2. In: CARLSON, K. J. and MARCHI, D. (eds) *Reconstructing Mobility: Environmental, Behavioural, and Morphological Determinants*. Springer. New York. United States of America.
- RUTA, M., BOTHA-BRINK, J., MITCHELL, S. A. and BENTON, M. J. 2013. The radiation of cynodonts and the ground plan of mammalian morphological diversity. *Proceedings of the Royal Society Biological Sciences* **280**: 1-10.
- SANCHEZ-VILLAGRA, M. R., MENKE, P. R. and GEISLER, J. H. 2004. Patterns of evolutionary transformation in the humerus of moles (Talpidae, Mammalia): a character analysis. *Mammal Study* **29**: 163-170.
- SHAH, R. K., TRIVDEI, B. D., PATEL, J. P., SHAH, G. V. and NIRVANI, A. B. 2006. A study of angle of humeral torsion. *Journal of the Anatomical Society of India* **55**: 43-47.
- SIDOR, C. A. and SMITH, R. M. H. 2004. A new galesaurid (Therapsida: Cynodontia) from the lower Triassic of South Africa. *Palaeontology* **47**: 535-556.
- SPECHT, M., LEBRUN, R. and ZOLLIKOFER, C. P. E. 2007. Visualizing shape transformation between chimpanzee and human braincases. *Vis Comput* **23**: 743-751.
- SOLOMON, E. P., BERG, L. R. and MARTIN, D. W. 2011. *Biology*. Brooks/Cole. Cengage Learning. Canada.
- SZALAY, F. S. 1994. *Evolutionary history of the marsupials and an analysis of osteological characters*. Cambridge University Press. New York. USA.
- TURNBULL, W. D. and REED, C. A. 1967. *Pseudochrysochloris*, a specialised burrowing mammal from the Early Oligocene of Wyoming. *Journal of Palaeontology* **41**: 623-631.

- VIZCAINO, S. F., FARINA, R. A. and MAZZETTA, G. 1999. Ulnar dimensions and fossoriality in armadillos and other South American mammals. *Acta Theriologica* **44**: 309-320.
- VIZCAINO, S.F. and MILNE, N. 2002. Structure and function in armadillo limbs (Mammalia: Xenarthra: Dasypodidae). *Journal of Zoology* **257**: 117-127.
- WARBURTON, N. M., GREGOINE, L., JACQUES, S. and FLANDRIN, C. 2013. Adaptations for digging in the forelimb muscle anatomy of the Southern brown bandicoot (*Isodon obesulus*) and bilby (*Macrotis lagotis*). *Australian Journal of Zoology* **61**: 402-419.
- ZELDITCH, M. L., SWIDERSKI, D. L., SHEETS, H. D. and FINK, W. L. 2004. *Geometric morphometrics for biologists*. Elsevier Academic Press. Kirkwood. New York. United States of America.

Appendix 1

Table A1: The functional indices (SMI, HRI, EI, IFA and URI) calculated for the forelimb by measurement of the DLH, HL, TDH, DEH, OL, FUL and TDU.

Species	Specimen number *	DLH (mm)	HL (mm)	SMI (%)	TDH (mm)	HL (mm)	HRI (%)	DEH (mm)	HL (mm)	EI (%)	OL (mm)	FUL (mm)	IFA (%)	TDU (mm)	FUL (mm)	URI (%)
<i>Thrinaxodon</i>	BPI7199	18.95	34.58	54.80	5.30	34.58	15.33	18.30	34.58	52.92	0.62	30.09	2.06	2.09	30.09	6.95
** <i>Cynognathus</i> (small)	BPI1675	-	-	-	-	-	-	-	-	-	2.30	81.29	2.83	7.38	81.29	9.08
** <i>Cynognathus</i> (large)	BPI1675	56.12	94.36	59.47	12.42	94.36	13.16	47.47	94.36	50.31	5.04	139.92	3.60	13.51	139.92	9.66
<i>Cistecephalus</i>	BPI2915	10.63	26.21	40.56	3.83	26.21	14.61	13.13	26.21	50.10	2.46	30.94	7.95	3.91	30.94	12.64
<i>Vombatus ursinus</i>	M10000	77.09	127.63	60.40	14.44	127.63	11.31	54.85	127.63	42.98	31.39	153.84	20.40	12.19	153.84	7.92
<i>Lasiorhinus kreffti</i>	J14051	76.93	125.58	61.26	21.87	125.58	17.42	58.39	125.58	46.50	33.52	155.35	21.58	9.88	155.35	6.36
<i>Vombatus ursinus</i>	A1258	64.55	107.36	60.12	17.69	107.36	16.48	46.07	107.36	42.91	32.37	140.08	23.11	13.37	140.08	9.54
<i>Varanus niloticus</i>	VN1	17.45	55.28	31.57	6.53	55.28	11.81	20.54	55.28	37.16	1.24	47.88	2.59	3.26	47.88	6.81
<i>Varanus niloticus</i>	VN2	20.27	56.13	36.11	5.56	56.13	9.91	18.88	56.13	33.64	0.65	50.75	1.28	2.82	50.75	5.56
<i>Crocodylus moreletti</i>	R 8 047	6.34	22.70	27.93	2.22	22.70	9.78	4.71	22.70	20.75	0.46	17.15	2.68	1.38	17.15	8.05
<i>Crocodylus</i>	ZA913	56.96	144.47	39.43	17.87	144.47	12.37	40.33	144.47	27.92	6.61	101.70	6.50	10.33	101.70	10.16

<i>Crocodylus niloticus</i>	TMS150	6.68	21.59	30.94	2.12	21.59	9.82	5.04	21.59	23.34	0.57	15.88	3.59	1.15	15.88	7.24
<i>Cordylus giganteus</i>	R 39 384	6.46	25.55	25.28	2.38	25.55	9.32	7.47	25.55	29.24	0.51	20.76	2.46	1.24	20.76	5.97
<i>Cordylus giganteus</i>	TMS133	7.78	30.13	25.82	2.83	30.13	9.39	8.98	30.13	29.80	0.58	23.74	2.44	1.30	23.74	5.48
<i>Cordylus giganteus</i>	TMS137	5.71	23.83	23.96	2.19	23.83	9.19	6.89	23.83	28.91	0.62	18.62	3.33	0.96	18.62	5.16
<i>Gerrhosaurus validus</i>	R 44 579	1.86	11.38	16.34	1.08	11.38	9.49	3.95	11.38	34.71	0.39	7.81	4.99	0.60	7.81	7.68
<i>Anolis equestris</i>	R 59 327	0.94	8.13	11.56	0.60	8.13	7.38	1.93	8.13	23.74	0.14	5.71	2.45	0.38	5.71	6.65
<i>Anolis equestris</i>	R 59 328	0.72	7.32	9.84	0.58	7.32	7.92	1.77	7.32	24.18	0.31	5.51	5.63	0.34	5.51	6.17
<i>Cordylus warreni</i>	R 45 805	3.67	16.92	21.69	1.33	16.92	7.86	5.04	16.92	29.79	0.51	12.59	4.05	0.68	12.59	5.40
<i>Platysaurus imperator</i>	R 67 614	5.01	23.62	21.21	1.99	23.62	8.43	5.32	23.62	22.52	0.66	17.07	3.87	0.76	17.07	4.45
<i>Pseudocordylus melanotus</i>	R 184 420	2.80	12.97	21.59	1.08	12.97	8.33	3.37	12.97	25.98	0.14	9.71	1.44	0.45	9.71	4.63
<i>Pseudocordylus melanotus</i>	TMS143	3.86	16.09	23.99	1.42	16.09	8.83	4.73	16.09	29.40	0.23	12.03	1.91	0.71	12.03	5.90

*Key for collection: BPI - Evolutionary Studies Institute collection at the University of the Witwatersrand (South Africa); VN - Animal, Plants and Environmental Sciences Museum collection at the University of the Witwatersrand (South Africa); ZA - School of Anatomical Sciences collection at the University of the Witwatersrand (South Africa); TMS - Ditsong National Museum of Natural History collection (South Africa); R - Museum of Comparative Zoology collection at Harvard University (Massachusetts); M - Australian National Wildlife Collection (Canberra); A - Queensland Museum (Brisbane); J - Tasmanian Museum collection (Hobart).

**Note: Two different sized *Cynognathus* were used for the study, however, it shares the same specimen number due to the forelimb elements being discovered at the same site and was labeled accordingly.

Shoulder Moment Index (SMI) is defined as the humeral deltoid length (DLH) divided by the humeral functional length [(DLH/HL) x 100]; Humerus Robustness Index (HRI) is defined as the humerus transverse diameter (TDH) divided by the humeral functional length [(TDH/HL) x 100]; Epicondyle Index (EI) is defined as the width of the epicondyle (DEH) divided by the humeral functional length [(DEH/HL) x 100]; Index of Fossorial Ability (IFA) is defined by the olecranon length (OL) divided by the ulna functional length [(OL/FUL) x 100]; Ulna Robustness Index (URI) is defined as the ulna transverse diameter (TDU) divided by the ulna functional length [(TDU/FUL) x 100] follows Elissamburu and Vizcaino (2004) and Elissamburu and De Santis (2011).

Table A2: Cross-sectional properties for humerii at their 50% region of interest.

Species	Specimen Number *	Ps. Ar	Cortical Area (mm ²)	% Ct. Ar	Logged Moments of Area (mm ⁴)**		Principal Angle (Θ)	Logged Principal moments of area (mm ⁴)**		I _y /I _x	I _{max} /I _{min}	Logged J (mm ⁴)**	J/2
					I _x	I _y		I _{max}	I _{min}				
<i>Thrinaxodon liorhinus</i>	BPI5558	279,80	251,16	89,76	5,31	5,47	56,97	5,21	5,60	1,03	0,93	10,81	5,41
<i>Cynognathus</i>	BPI1675	161,27	79,24	49,13	11,00	10,31	25,09	10,18	11,32	0,94	0,90	21,50	10,75
<i>Cistecephalus</i>	BPI2915	177,76	142,16	79,97	5,13	5,52	82,64	5,13	5,53	1,08	0,93	10,65	5,33
<i>Vombatus ursinus</i>	M10000	232,88	175,19	75,23	10,35	11,27	66,47	10,21	11,71	1,09	0,87	21,92	10,96
<i>Lasiorhinus kreffti</i>	J14051	295,22	263,62	89,29	9,97	10,50	57,37	9,72	11,15	1,05	0,87	20,87	10,44
<i>Vombatus ursinus</i>	A1258	219,59	196,52	89,49	9,59	10,94	75,04	9,53	11,19	1,14	0,85	20,73	10,36
<i>Varanus niloticus</i>	VN1	134,64	110,06	81,74	8,62	8,94	-61,47	8,51	9,11	1,04	0,93	17,62	8,81
<i>Varanus niloticus</i>	VN2	112,86	94,37	83,62	9,12	9,30	-59,51	9,03	9,41	1,02	0,96	18,44	9,22
<i>Crocodylus</i>	R 8 047	84,63	69,40	82,00	6,31	6,05	-8,05	6,04	6,31	0,96	0,96	12,35	6,18

<i>moreletti</i>														
<i>Crocodylus</i>	ZA913	133,29	121,46	91,12	12,70	12,60	11,39	12,59	12,70	0,99	0,99	25,29	12,65	
<i>Crocodylus niloticus</i>	TMS150	115,91	71,00	61,26	5,49	5,45	42,25	5,31	5,67	0,99	0,94	10,97	5,49	
<i>Cordylus giganteus</i>	R 39 384	89,46	60,78	67,94	6,64	6,58	-38,14	6,49	6,75	0,99	0,96	13,24	6,62	
<i>Cordylus giganteus</i>	TMS133	92,89	59,98	64,57	7,27	7,14	-35,10	7,02	7,42	0,98	0,95	14,44	7,22	
<i>Cordylus giganteus</i>	TMS137	80,79	54,83	67,87	6,67	6,40	-22,82	6,35	6,73	0,96	0,94	13,08	6,54	
<i>Gerrhosaurus validus</i>	R 44 579	108,83	95,47	87,72	2,96	2,84	-16,77	2,83	2,97	0,96	0,95	5,80	2,90	
<i>Anolis equestris</i>	R 59 327	57,68	41,68	72,26	3,02	2,77	-1,79	2,77	3,02	0,92	0,92	5,78	2,89	
<i>Anolis equestris</i>	R 59 328	67,21	56,21	83,63	2,17	2,04	-2,64	2,04	2,17	0,94	0,94	4,21	2,11	
<i>Cordylus warreni</i>	R 45 805	82,34	72,74	88,34	5,05	5,02	-33,90	4,99	5,08	0,99	0,98	10,07	5,03	
<i>Platysaurus imperator</i>	R 67 614	93,10	70,97	76,23	6,19	6,23	-49,52	6,09	6,34	1,01	0,96	12,44	6,22	
<i>Pseudocordylus melanotus</i>	R184 420	73,62	69,58	94,52	4,19	4,16	-41,59	4,06	4,31	0,99	0,94	8,37	4,19	
<i>Pseudocordylus melanotus</i>	TMS143	86,17	64,64	75,02	4,81	4,76	-40,10	4,64	4,95	0,99	0,94	9,60	4,80	

*Key for collection: BPI - Evolutionary Studies Institute collection at the University of the Witwatersrand (South Africa); VN - Animal, Plants and Environmental Sciences Museum collection at the University of the Witwatersrand (South Africa); ZA - School of Anatomical Sciences collection at the University of the Witwatersrand (South Africa); TMS - Ditsong National Museum of Natural History collection (South Africa); R - Museum of Comparative Zoology collection at Harvard University (Massachusetts); M - Australian National Wildlife Collection (Canberra); A - Queensland Museum (Brisbane); J - Tasmanian Museum collection (Hobart).

** I_x , I_y , I_{max} , I_{min} and J were calculated by taking the natural log of the variable divided by length to the fourth power.

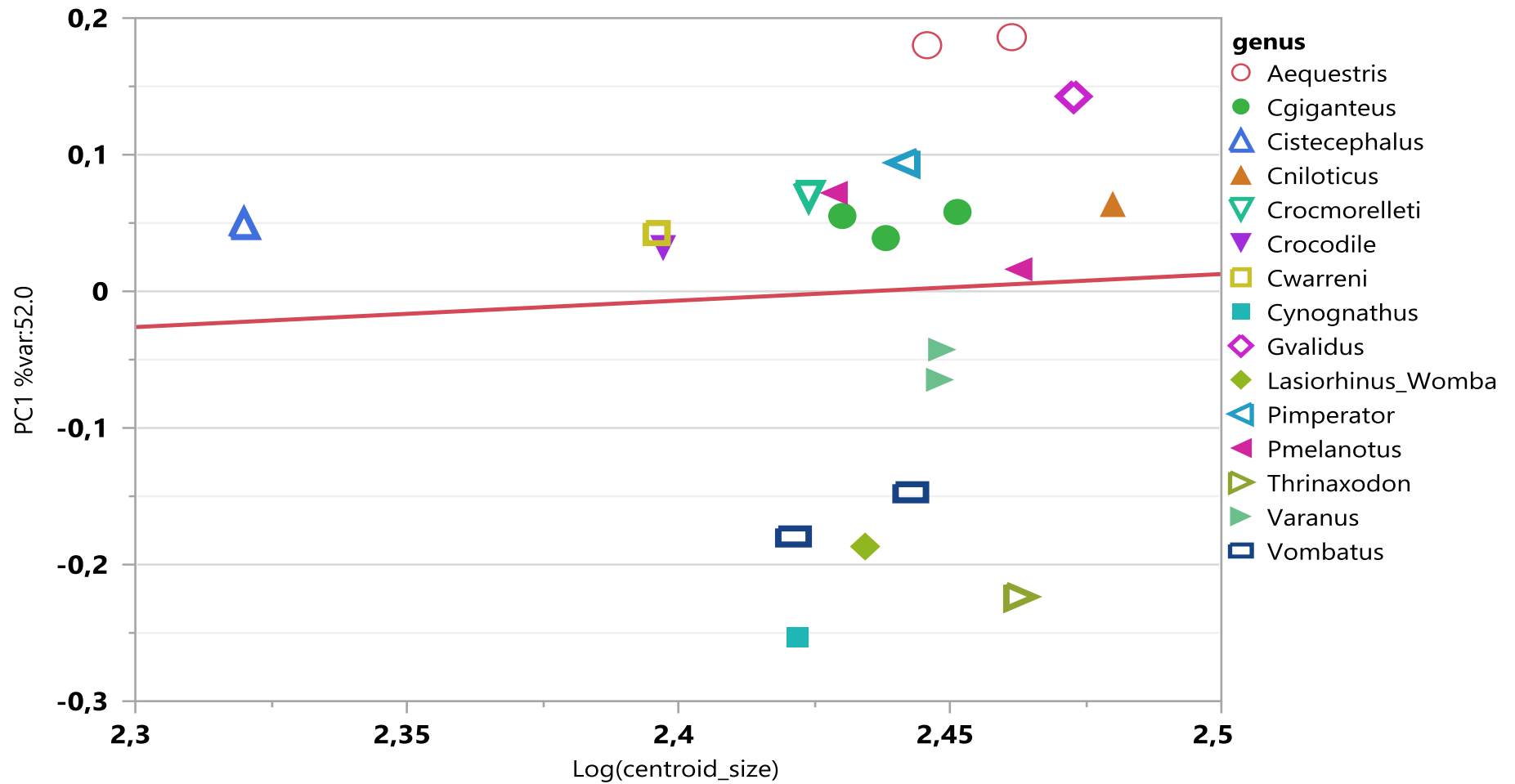


Figure A1: Regression of PC1 vs. in humerus centroid size, with equation $PC1 \%var: 52.03 = -0.473 + 0.194 * Log(centroid_size)$, $r^2 = 0.003$, $p > 0.825$

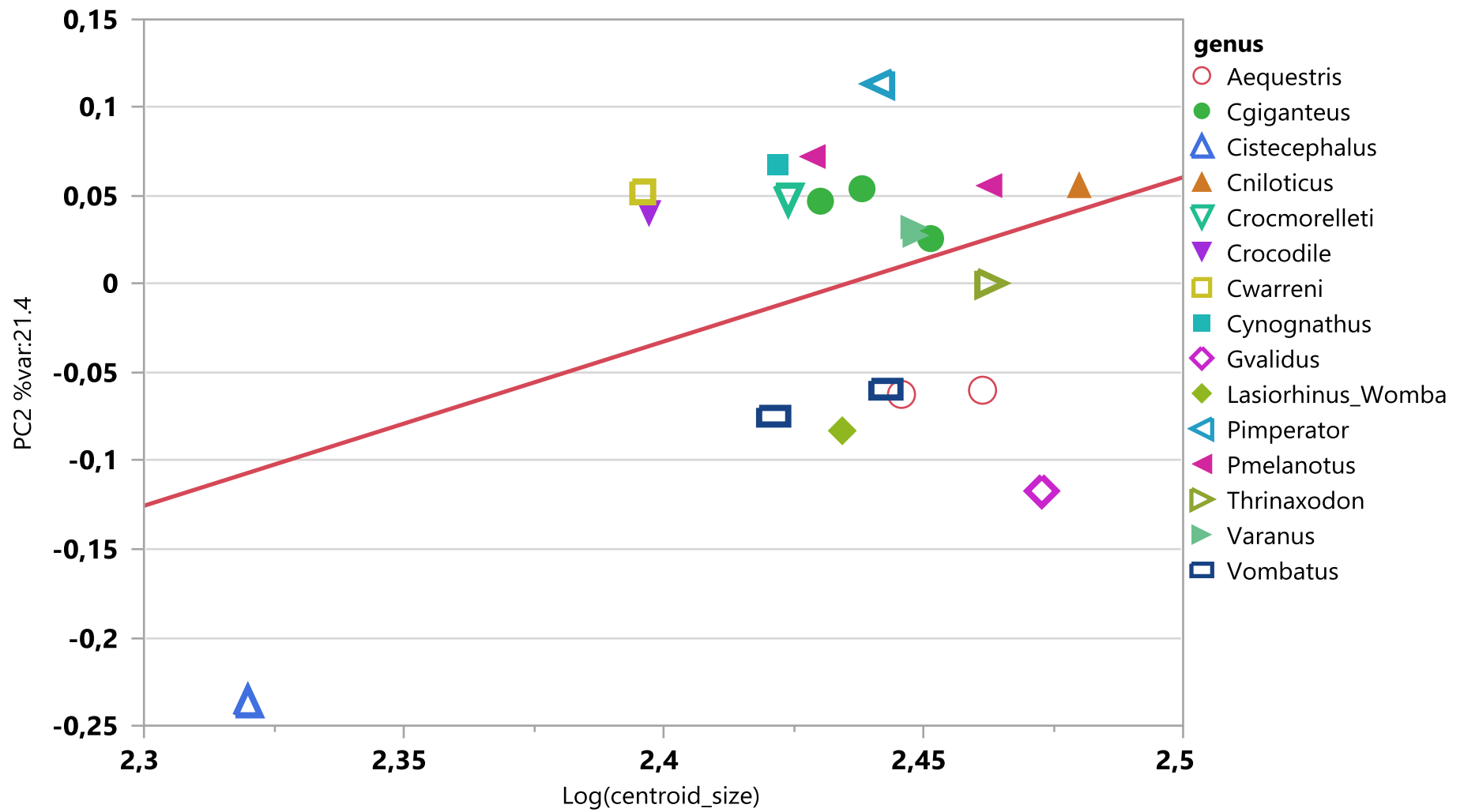


Figure A2: Regression of PC2 vs. in humerus centroid size, with equation $PC2 \%var: 21.40 = -2.265 + 0.930 * Log(centroid_size)$, $r^2 = 0.148$, $p > 0.085$

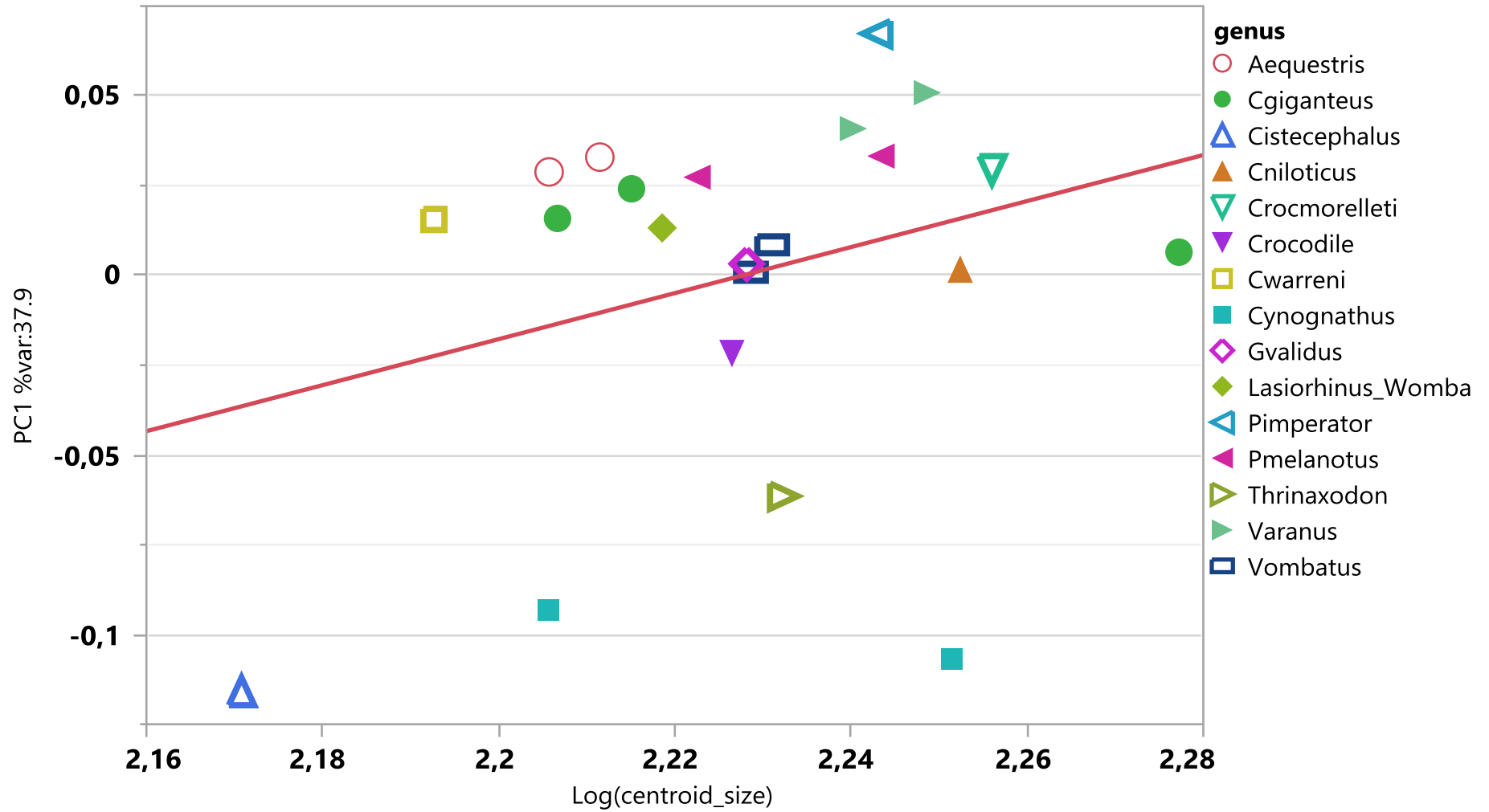


Figure A3: Regression of PC1 vs. in radius centroid size, with equation $PC1 \%var: 37.92 = -1.428 + 0.641 * \text{Log}(\text{centroid_size})$, $r^2 = 0.094$, $p > 0.166$

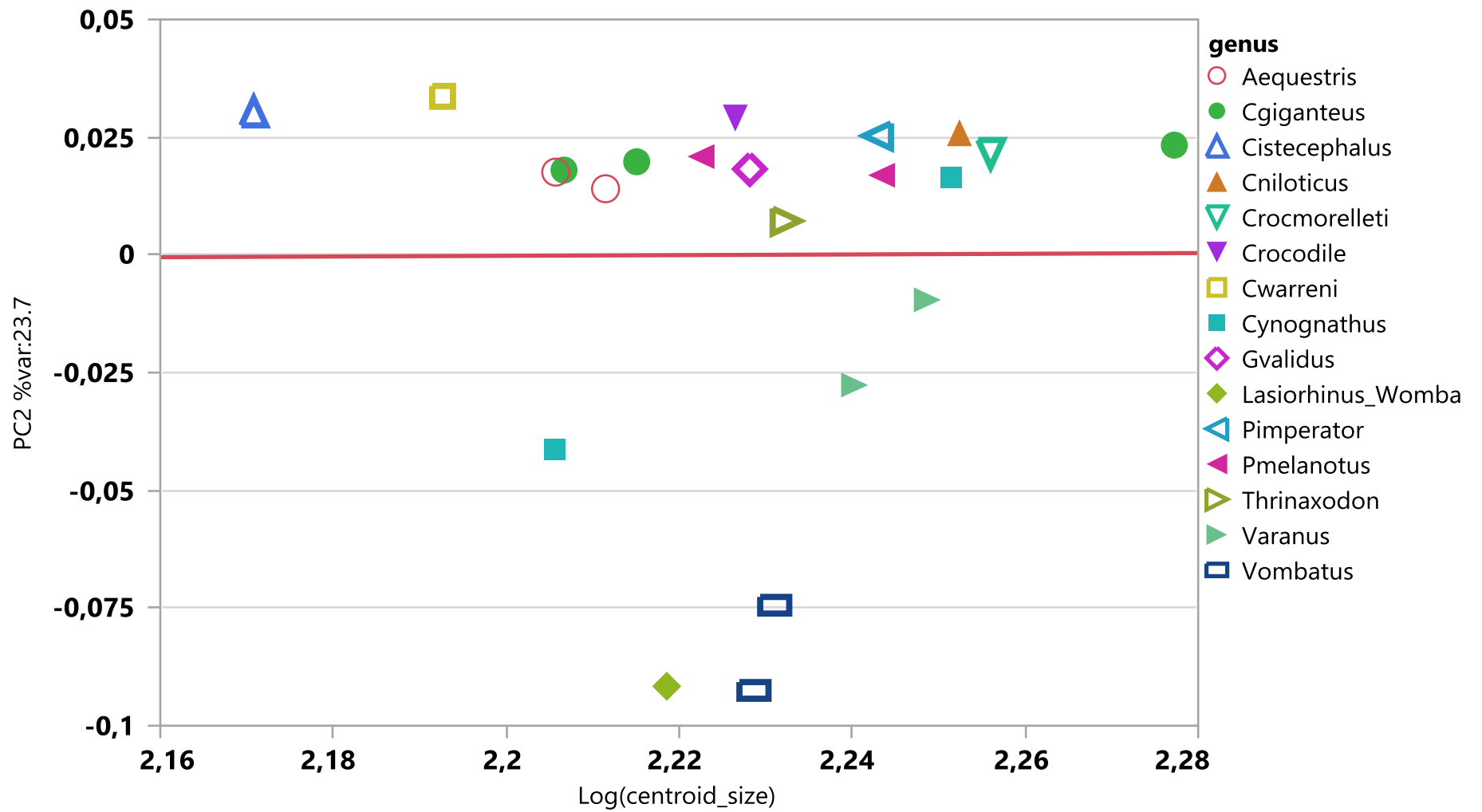


Figure A4: Regression of PC2 vs. in radius centroid size, with equation $PC2 \% \text{ var: } 23.70 = -0.016 + 0.007 * \text{Log}(\text{centroid_size})$, $r^2 = 0$, $p > 0.985$

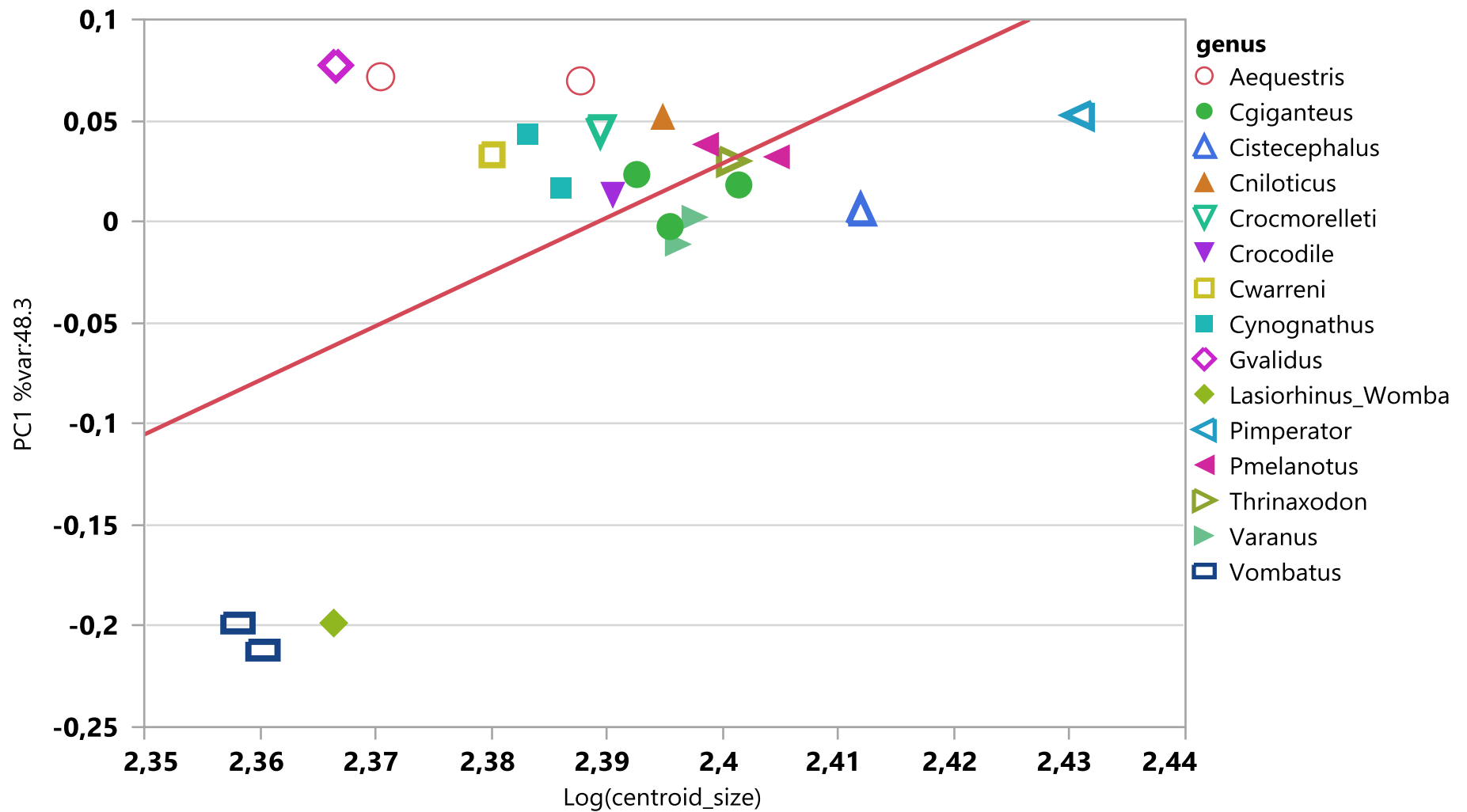


Figure A5: Regression of PC1 vs. in ulna centroid size, with equation $PC1 \%var: 48.38 = -6.409 + 2.683 * \text{Log}(\text{centroid_size})$, $r^2 = 0.046$, $p < 0.009$

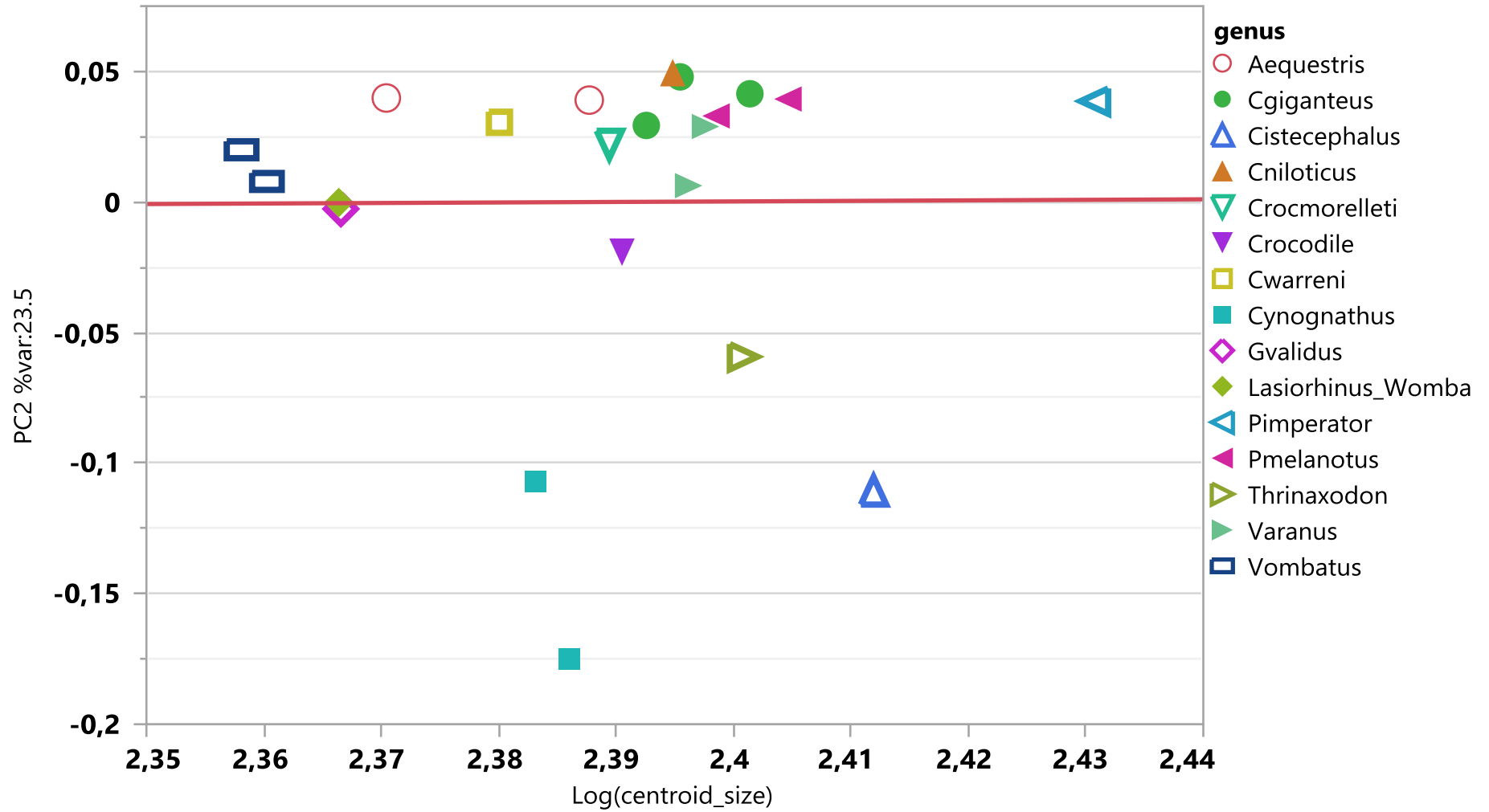


Figure A6: Regression of PC2 vs. in ulna centroid size, with equation $PC2 \%var: 23.51 = -0.048 + 0.020 * \text{Log}(\text{centroid_size})$, $r^2 = 0$, $p > 0.979$

Appendix 2

List of Landmarks

Table A3: Humeral landmarks for taxa in the study.

Element	View*	Position
Head	Anterior	1. Head anterior most
	Posterior	2. Head posterior most
	Superior	3. Head lateral
	Superior	4. Head medial
	Anterior	5. Head central of the articulating surface
Tuberosity	Superior	6. Lesser tuberosity dorsal (Posterior)
	Superior	7. Lesser tuberosity ventral (Anterior)
	Superior	8. Greater tuberosity posterior (dorsal)
	Superior	9. Greater tuberosity anterior (Ventral)
Deltopectoral crest	Lateral	10. Deltopectoral crest proximal (Under the head)
	Lateral	11. Deltopectoral crest tip (Highest point)
	Lateral	12. Deltopectoral crest contact with diaphysis (Lowest point)
Bicipital groove	Superior	13. Proximal point bicipital groove
Entepicondylar	Medial	14. Entepicondyle dorsal margin (Posterior projection)
	Medial	15. Entepicondyle ventral margin (Anterior)
	Medial	16. Contact of disto-medial-dorsal crest (Shaft meets the curvature) – which start in the entepicondyle
Ectepicondylar	Lateral	17. Ectepicondyle dorsal margin (Posterior – Above capitulum)
	Lateral	18. Ectepicondyle ventral margin (Anterior – above capitulum)
	Lateral	19. Proximal point of the disto-lateral crest (At the end of the crest)
Distal articulation condyle	Inferior	20. Distal articulation anterior (ventral-lateral)
	Inferior	21. Distal articulation anterior (ventral-medial)
	Inferior	22. Distal articulation posterior (dorsal-lateral)
	Inferior	23. Distal articulation posterior (dorsal-medial)
Trochlea	Inferior	24. Distal articulation anterior
	Inferior	25. Distal articulation posterior
	Inferior	26. Distal articulation deepest point
Diaphysis	Posterior	27. Mid shaft posterior
	Lateral	28. Mid shaft lateral
	Medial	29. Mid shaft medial

*The view column represents the orientation of the bone when positioning landmarks.

Table A4: Radial landmarks for taxa in the study.

Element	View*	Position
Head (Proximal end)	Superior	1. Posterior margin
	Superior	2. Anterior margin
	Superior	3. Lateral margin
	Superior	4. Medial margin

	Superior	5. Central of the articulating surface
Radial tuberosity		6. Central point
Distal articular surface	Inferior	7. Posterior margin
	Inferior	8. Anterior margin
	Inferior	9. Lateral margin
	Inferior	10. Medial margin
Diaphyseal location from proximal end		11. Posterior margin of the 50% length
		12. Anterior margin of the 50% length
		13. Lateral margin of the 50% length
		14. Medial margin of the 50% length
		15. Posterior margin of the 75% length
		16. Anterior margin of the 75% length
		17. Lateral margin of the 75% length
		18. Medial margin of the 75% length

*The view column represents the orientation of the bone when positioning landmarks.

Table A5: Ulnar landmarks for taxa in the study.

Element	View*	Position
Olecranon	Superior	1. Posterior margin
	Superior	2. Anterior margin
	Superior	3. Lateral (Radial notch)
	Superior	4. Medial margin
Ulna-Trochlea notch	Medial	5. Proximal anconeal process tip
	Medial	6. Articulation deepest point
	Medial	7. Distal point on keel of articulation
	Medial	8. Lateral most margin
	Medial	9. Medial most margin
Radial-Ulna notch	Lateral	10. Tip of radial notch - Lateral most margin
	Lateral	11. Medial most margin
Distal articular surface	Inferior	12. Posterior margin
	Inferior	13. Anterior margin
	Inferior	14. Lateral margin
	Inferior	15. Medial margin
Diaphyseal location from proximal end		16. Posterior margin of the 50% length
		17. Anterior margin of the 50% length
		18. Lateral margin of the 50% length
		19. Medial margin of the 50% length
		20. Posterior margin of the 75% length
		21. Anterior margin of the 75% length
		22. Lateral margin of the 75% length
	23. Medial margin of the 75% length	

*The view column represents the orientation of the bone when positioning landmarks.

Appendix 3

Muscles

From the dissection of the reptile, *Crocodylus*, the muscle attachment for *Thrinaxodon* was inferred with reference to the muscle scars that were observed during segmentation and landmark analyses of the forelimb. References used for interpretation were Grand and Barboza (2001), Meers (2003) and Abdala and Diogo (2010). However, it is noteworthy to state that *Thrinaxodon* being a mammal-like reptile, is similar in forelimb structure to reptiles but shares similarity to mammals in their muscle attachment. The muscle actions were inferred from the morphological perspective rather than the physiological aspect.

M. latissimus dorsi which originates from the thoracodorsal fascia of the vertebrae, inserts on the lateral side of the humeral head (Figure A7). This muscle is an extensor and retracts the humerus dorsally.

M. subscapularis is a stabiliser of the shoulder and originates on the medial surface of the scapula. This muscle inserts on the articular capsule of the humerus.

M. scapulohumeralis caudalis originates from the caudal region of the scapula and inserts on the proximal end of the humerus by convergence (Figure A7). It elevates and protracts the humerus as well as stabilises the glenohumeral joint.

M. deltoideus scapularis takes its origin from the lateral surface of the scapula and inserts on the lateral side of the proximal end of the humerus. This muscle acts as a stabiliser of the shoulder joint and abducts the humerus. *M. deltoideus clavicularis* originates on the cranial margin of the scapula and inserts on the deltopectoral crest (Figure A7). It protracts the humerus and is a flexor of the forearm.

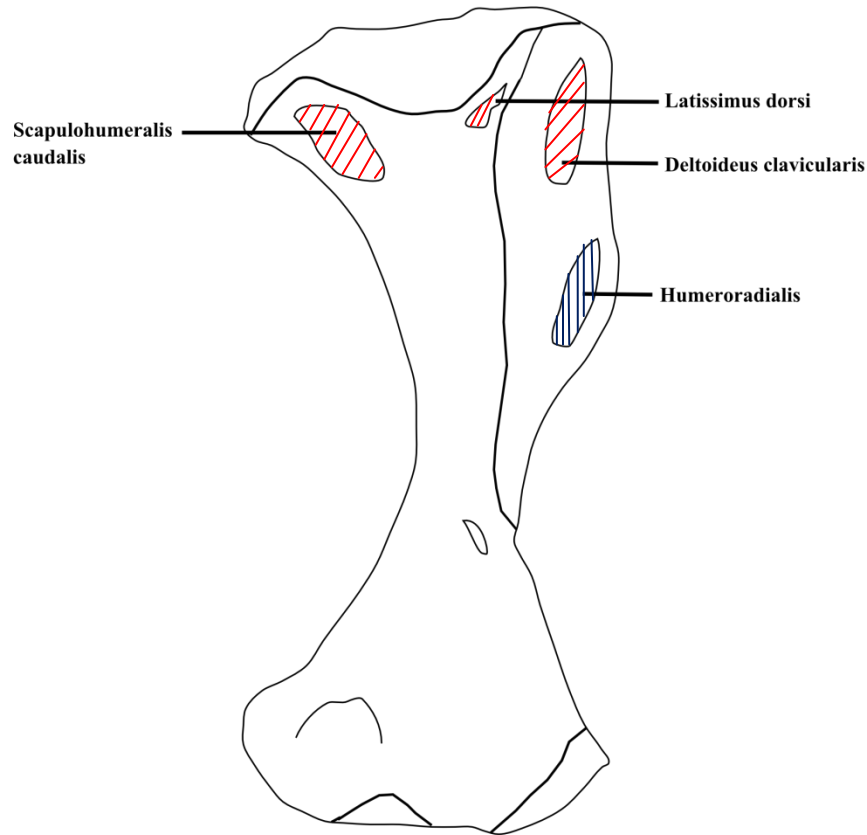



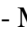



Figure A7: Posterior view of *Thrinaxodon* humerus with muscle scars that were visible during analyses.     - Muscle Origin and  - Muscle Insertion.

M. triceps brachii consists of five muscle heads which are the *m. triceps longus lateralis*, *m. triceps longus caudalis*, *m. triceps brevis cranialis*, *m. triceps brevis intermedius* and *m. triceps brevis caudalis*. The *m. triceps brachii* flexes the brachium and extends the antebrachium, which aids in support of the reptilian flexed-limb posture. *M. triceps longus* muscles originate on the scapula and converge to insert on the ulna (Figure A10). *M. triceps brevis cranialis* and *m. triceps brevis caudalis* originate from the humeral head and insert into the deep tendons on the lateral epicondyle (Figure A8).

M. pectoralis originates on three different parts of the sternum and converges to insert on the deltopectoral crest of the humerus (Figure A8). It is a powerful ventral flexor and adductor that is responsible for retracting the humerus. Consequently, *m. pectoralis* has an important role in maintaining flexed limb posture in reptiles (Meers 2003).

M. supracoracoideus longus is a muscle that protracts and adducts the humerus with an origin on the cranial surface of the scapula and an insertion on the apex of the deltopectoral crest of the humerus.

M. supracoracoideus brevis which originates from the acromion, inserts on the deltopectoral crest of the humerus and protracts as well as adducts the humerus.

M. coracobrachialis brevis ventralis originates from the coracoids and inserts on the deltopectoral crest slightly distally on the humeral shaft (Figure A8). This muscle flexes the shoulder joint, and retracts and adducts the humerus. *M. coracobrachialis brevis dorsalis* contributes to protracting and flexing the forelimb. It acts as a primary stabiliser of the head of the humerus in the glenoid. It has an origin on the scapula and converges to insert on the articular capsule slightly distal to the head of the humerus.

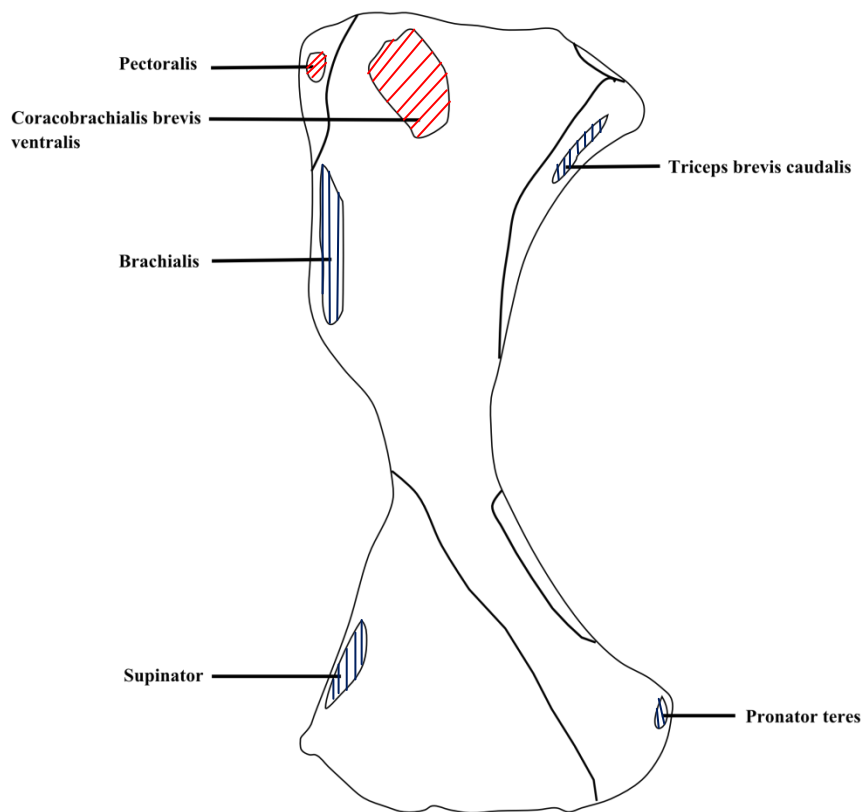


Figure A8: Anterior view of *Thrinaxodon* humerus with muscles scars that were visible during analyses. □□□□ - Muscle Origin and ▨ - Muscle Insertion.

M. Brachialis is a flexor of the antebrachium, and originates distal to the deltopectoral crest of the humerus and inserts on the radius together with the biceps tendon (Figure A8). The *m. biceps brachii* flexes the antebrachium and extends the humerus. This muscle originates on the coracoid and inserts between the radial head and the radial tuberosity.

The *m. humeroradialis* leaves a scar on the ventral surface of the humerus with an origin from the proximal end of the humerus (Figure A7) and an insertion on the proximal end of the radius (Figure A9). This muscle flexors the antebrachium.

The *m. teres major* elevates the humerus, originates on the lateral surface of the scapula and inserts on the humerus proximally opposite the deltopectoral crest.

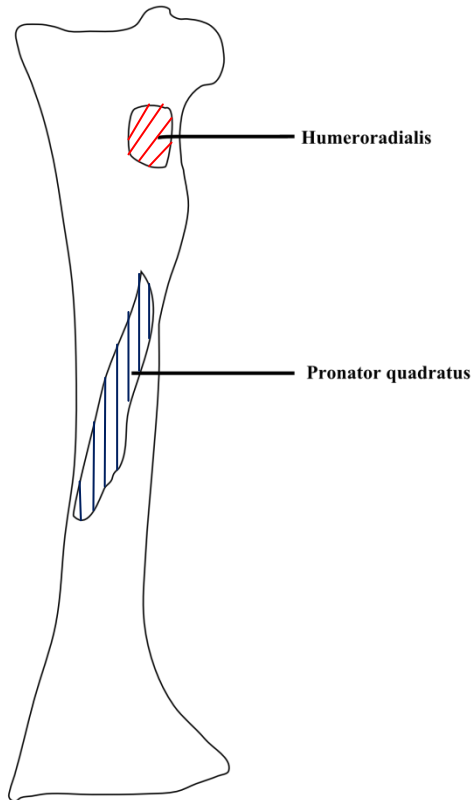


Figure A9: Anterior view of *Thrinaxodon* radius with muscles scars that were visible during analyses. □□□□ - Muscle Origin and ▨ - Muscle Insertion.

The *m. supinator* of the antebrachium originates from the epicondyle of the humerus (Figure A8) and inserts on the shaft of the radius.

M. extensor carpi radialis longus and *m. extensor carpi ulnaris longus* originate on opposite ends of the humeral epicondyles and insert in the wrist. The *m. extensor carpi radialis brevis* extends the wrist and adducts the hand. The extensor muscles originate on the lateral surface of the forelimb and insert on

its medial surface, whereas the flexor muscles originate on the medial surface and insert on its lateral surface.

M. Flexor carpi ulnaris originates on the epicondyle of the humerus and inserts on the wrist. The *m. flexor digitorum longus* consists of *m. flexor digitorum longus pars humeri*, *m. flexor digitorum longus pars ulnaris* and *m. flexor digitorum longus pars carpalis*. These muscles take their origin from the epicondyle of the humerus, the ulna head and distal end of the ulna. It inserts and flexes the wrist and hand.

The *m. pronator teres* originates on the epicondyle of the humerus (Figure A8) and inserts on the shaft of the radius. This muscle pronates the antebrachium while flexing the radiohumeral joint which maintains the sprawling posture. *M. pronator quadratus* pronates and stabilises the antebrachium. It originates on the shaft of the radius (Figure A9) and inserts on the shaft of the ulna (Figure A10).

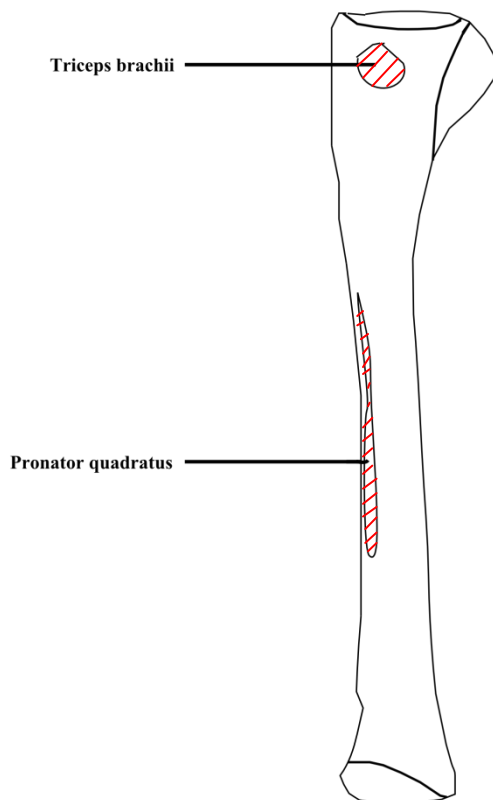


Figure A10: Posterior view of *Thrinaxodon* ulna with muscles scars that were visible during analyses. □□□□ - Muscle Origin and ▨ - Muscle Insertion.